ARTICLE

LKB1 orchestrates dendritic cell metabolic quiescence and anti-tumor immunity

Yanyan Wang[1], Xingrong Du [1], Jun Wei[1], Lingyun Long[1], Haiyan Tan[2,3], Cliff Guy[1], Yogesh Dhungana[1], Chenxi Qian[1,4], Geoffrey Neale[5], Yang-Xin Fu [6], Jiyang Yu[4], Junmin Peng[2,3] and Hongbo Chi [1]

Dendritic cells (DCs) play a pivotal role in priming adaptive immunity. However, the involvement of DCs in controlling excessive and deleterious T cell responses remains poorly defined. Moreover, the metabolic dependence and regulation of DC function are unclear. Here we show that LKB1 signaling in DCs functions as a brake to restrain excessive tumor-promoting regulatory T cell (Treg) and Th17 cell responses, thereby promoting protective anti-tumor immunity and maintaining proper immune homeostasis. LKB1 deficiency results in dysregulated metabolism and mTOR activation of DCs. Loss of LKB1 also leads to aberrant DC maturation and production of cytokines and immunoregulatory molecules. Blocking mTOR signaling in LKB1-deficient DCs partially rectifies the abnormal phenotypes of DC activation and Treg expansion, whereas uncontrolled Th17 responses depend upon IL-6–STAT3 signaling. By coordinating metabolic and immune quiescence of DCs, LKB1 acts as a crucial signaling hub in DCs to enforce protective anti-tumor immunity and normal immune homeostasis.

INTRODUCTION

Dendritic cells (DCs) bridge the innate and adaptive immune systems and play important roles in mediating protective immune responses against pathogens and tumors. Despite our understanding of the innate and adaptive functions of DCs, their importance in immune homeostasis is less understood. Under steady state, DCs express low levels of maturation markers and cytokines,[1,2] although whether and how this quiescent state of DCs is actively maintained are unclear. The specific deletion of DCs via genetic approaches causes spontaneous inflammation and autoimmune diseases,[3–5] supporting the crucial roles of DCs in maintaining immune homeostasis. DCs are key mediators of peripheral tolerance, in part, by promoting the differentiation and expansion of regulatory T cells (Tregs).[6,7] Tregs play important roles in immune tolerance and suppression, and the size of the Treg pool is a critical component of immune homeostasis. Tregs can be divided into thymus-derived Tregs (tTregs) and peripherally derived Tregs (pTregs) based on their developmental origins.[8] Whereas it is well recognized that DCs promote pTreg conversion from naïve T cells,[6,7] how DCs maintain tTreg homeostasis,[9] especially the inhibitory pathways that limit excessive and deleterious tTreg expansion, is not fully understood.

Emerging studies highlight the importance of metabolic reprograming of DCs for their functional activation to prime T cell responses.[10,11] Signaling pathways including PI3K-AKT and TBK1-IKKε have been shown to drive DC metabolism upon activation by Toll-like receptors.[12,13] However, the inhibitory pathways that restrict DC metabolism are not well understood.

The tumor suppressor liver kinase B1 (LKB1), which is encoded by *Stk11*, is a serine/threonine kinase and is responsible for the Peutz-Jeghers Syndrome.[14] Functioning through 14 downstream kinases of the 5'AMP-activated protein kinase (AMPK) family, LKB1 plays important roles in regulating cell growth, survival, and metabolism.[15] LKB1 is an essential regulator of hematopoietic stem cell metabolism and survival.[16–18] Recent studies also demonstrate that loss of LKB1 disrupts Treg survival and function[19–21] and induces T cell dysfunction and the development of gastrointestinal polyposis.[22,23] However, the role of LKB1 in metabolism and function of DCs remains to be explored.

To investigate the physiological function of LKB1 signaling in DCs, we developed a mouse model to delete LKB1 in CD11c-expressing cells, mainly DCs. Such genetic modulation promoted peripheral expansion of Tregs, mainly tTregs, as well as thymic Treg development. The accumulation of Tregs accelerated tumor growth, and Treg depletion partially reversed this phenotype. In addition, LKB1 deficiency in DCs enhanced tumor-promoting Th17 cell differentiation. Mechanistically, LKB1 deficiency led to dysregulated metabolism and mTOR activation, accompanied by enhanced DC maturation and uncontrolled production of cytokines and other immunoregulatory molecules. Suppressing mTOR signaling and IL-6–STAT3 signaling partially rectified the abnormal Treg expansion and Th17 responses, respectively. Our results identify LKB1 as a crucial signaling hub in DCs, necessary to maintain normal immune homeostasis and anti-tumor immunity.

[1]Department of Immunology, St. Jude Children's Research Hospital, Memphis, TN 38105, USA; [2]Departments of Structural Biology and Developmental Neurobiology, St. Jude Children's Research Hospital, Memphis, TN 38105, USA; [3]Center for Proteomics and Metabolomics, St. Jude Children's Research Hospital, Memphis, TN 38105, USA; [4]Department of Computational Biology, St. Jude Children's Research Hospital, Memphis, TN 38105, USA; [5]Hartwell Center for Bioinformatics and Biotechnology, St. Jude Children's Research Hospital, Memphis, TN 38105, USA and [6]Department of Pathology, University of Texas (UT) Southwestern Medical Center, Dallas, TX 75390, USA
Correspondence: Hongbo Chi (hongbo.chi@stjude.org)

RESULTS

LKB1 is activated in DCs in tumor, and its deletion in DCs impairs anti-tumor immunity

To examine the function of LKB1 in DCs, we crossed mice carrying floxed *Stk11* alleles (*Stk11*fl/fl) with CD11c-Cre mice[24] to generate LKB1[ΔDC] mice, which had efficient *Stk11* deletion and reduced protein abundance in CD11c-expressing DCs (Supplementary information, Fig. S1a). Since myeloid cells other than DCs can also express CD11c,[24] we also examined *Stk11* mRNA expression in macrophages but found very little *Stk11* deletion from LKB1[ΔDC] mice (Supplementary information, Fig. S1b). Flow cytometry analysis of splenic DC populations in LKB1[ΔDC] mice showed that percentages of conventional DCs (cDCs, CD11c^{hi}MHC-II$^+$) and plasmacytoid DCs (pDCs, CD11c^{lo}PDCA-1$^+$) were normal (Supplementary information, Fig. S1c, d). Within cDCs, the percentage of CD8α$^+$ subset was slightly increased, while that of CD8α$^-$ subset (CD11b$^+$) was reduced (Supplementary information, Fig. S1c, d). However, cell numbers of cDCs, pDCs, CD8α$^+$ and CD8α$^-$ cDCs in the spleen were all comparable between wild-type (WT) and LKB1[ΔDC] mice (Supplementary information, Fig. S1d). Next, we examined the effects of LKB1 deficiency in DCs on T and B cell compartments, and found that LKB1[ΔDC] mice had comparable frequencies of CD4$^+$ and CD8$^+$ T cells and B cells (Supplementary information, Fig. S1e). Thus, LKB1 deficiency does not affect the development of DCs, T cells and B cells.

LKB1 is a tumor suppressor, and loss of LKB1 in T cells results in the development of gastrointestinal polyposis.[22] To explore the regulation and function of DC LKB1 signaling in tumors, we inoculated WT mice with MC38 colon adenocarcinoma cells and analyzed the activation of LKB1 in DCs from tumor and spleen. Flow cytometry analysis showed that the phosphorylation of LKB1 was upregulated in tumor DCs compared with splenic DCs, whereas p38 phosphorylation was similar (Fig. 1a), suggesting that DCs upregulate LKB1 signaling pathway in tumors.

We next challenged LKB1[ΔDC] mice with MC38 tumor cells. Compared with WT mice, tumor growth was significantly increased in LKB1[ΔDC] mice (Fig. 1b). The same finding was also observed in the MC38-EGFR tumor model (Fig. 1c) and B16-OVA transplantable tumor model (Supplementary information, Fig. S1f). To examine whether this requires lymphocyte-dependent immune responses, we generated alymphoid LKB1[ΔDC]*Rag1*$^{-/-}$ and *Rag1*$^{-/-}$ chimeras, by transferring bone marrow cells from LKB1[ΔDC]*Rag1*$^{-/-}$ and littermate *Rag1*$^{-/-}$ control mice into *Rag1*$^{-/-}$ mice. After 8 weeks of reconstitution, the chimeras were inoculated with MC38 tumor cells. *Rag1*$^{-/-}$ and LKB1[ΔDC]*Rag1*$^{-/-}$ chimeras exhibited similar tumor growth (Fig. 1d), suggesting that the enhanced tumor growth in LKB1[ΔDC] mice requires the involvement of lymphocytes, possibly via DC-lymphocyte crosstalk.

We therefore isolated the tumor tissues to dissect the immune cell types involved in the tumor development. Analysis of tumor-infiltrating lymphocytes indicated increased Tregs in LKB1[ΔDC] mice compared with WT controls (Fig. 1e). Tregs in tumor-draining lymph nodes were also increased in LKB1[ΔDC] mice (Fig. 1e), suggesting that Tregs play important roles in accelerating tumor growth. Consistent with this notion, the important cytotoxic cytokine produced by intratumor T cells, IFNγ, was significantly suppressed in tumor-infiltrating CD4$^+$ T cells, but not CD8$^+$ T cells, in LKB1[ΔDC] mice (Supplementary information, Fig. S1g). To directly examine if the enhanced tumor growth in LKB1[ΔDC] mice was caused by Tregs, we bred LKB1[ΔDC] mice with mice expressing diphtheria toxin receptor (DTR) under the control of the *Foxp3* promoter[25] (LKB1[ΔDC]*Foxp3*[DTR]), which allows for the depletion of Foxp3-expressing Tregs upon diphtheria toxin treatment. We then transferred bone marrow cells from LKB1[ΔDC]*Foxp3*[DTR] mice and their littermate controls into *Rag1*$^{-/-}$ mice to generate chimeras. After challenge with MC38 tumor cells, diphtheria toxin-treated LKB1[ΔDC]*Foxp3*[DTR] chimeras had drastically decreased tumor growth compared with LKB1[ΔDC] mice (Fig. 1f). Altogether, loss of LKB1 in DCs induces increased Tregs in tumors, which contributes to tumor growth.

LKB1 deficiency in DCs results in increased tTreg accumulation

Based on the finding of increased Tregs in tumor-infiltrating lymphocytes of LKB1[ΔDC] mice, we analyzed Tregs
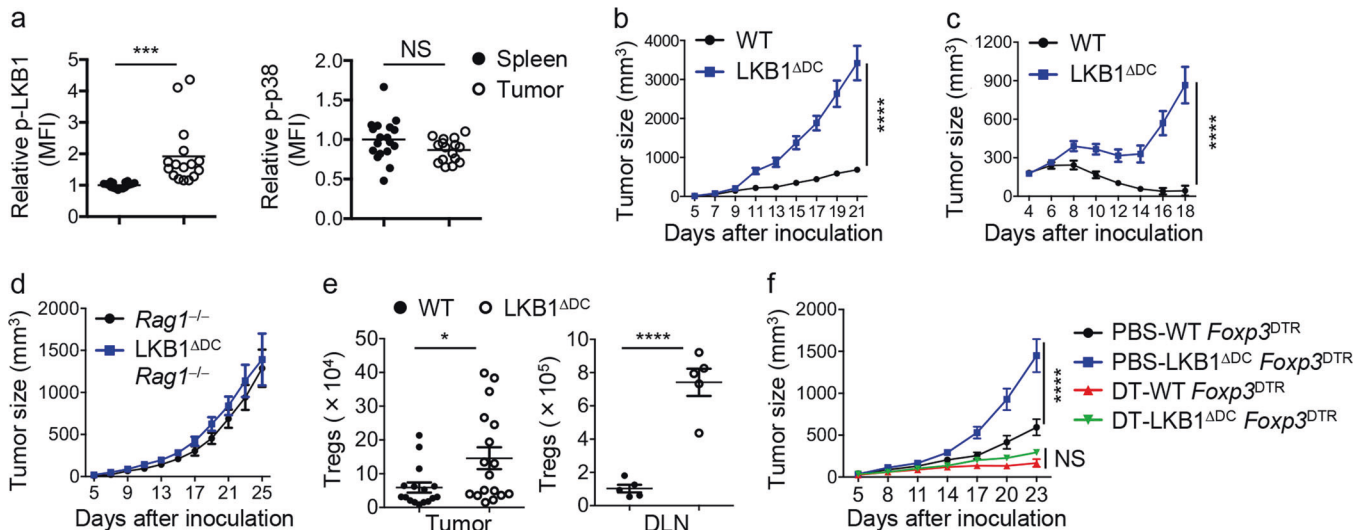

Fig. 1 LKB1 is activated in DCs in tumor, and its deletion in DCs impairs anti-tumor immunity. **a** C57BL/6 mice were inoculated with MC38 tumor cells for 14 days and DCs from tumor tissues and spleen were analyzed for p-LKB1 and p-p38 expression. **b, c** Tumor growth curve in wild-type (WT) and LKB1[ΔDC] mice following inoculation of MC38 tumor cells (b; WT, *n* = 12; LKB1[ΔDC] mice, *n* = 9) or MC38-EGFR cells (c; WT, *n* = 8; LKB1[ΔDC] mice, *n* = 9). **d** Sublethally irradiated *Rag1*$^{-/-}$ mice were reconstituted with control *Rag1*$^{-/-}$- or LKB1[ΔDC]*Rag1*$^{-/-}$-derived bone marrow cells for chimera generation, and subsequently inoculated with MC38 tumor cells for tumor growth curve. **e** Statistics of Treg numbers in tumor tissues and draining lymph nodes (DLN) of WT and LKB1[ΔDC] mice after inoculation of MC38 tumor cells for 13–14 days. **f** Sublethally irradiated *Rag1*$^{-/-}$ mice were reconstituted with control *Foxp3*[DTR]- or LKB1[ΔDC]*Foxp3*[DTR]-derived bone marrow cells for chimera generation, and subsequently treated with or without diphtheria toxin (DT), and inoculated with MC38 tumor cells for tumor growth curve (*n* = 10 per group). Data in plots indicate the means ± s.e.m; each symbol represents an individual mouse. *NS* not significant; *$P < 0.05$, ***$P < 0.001$, ****$P < 0.0001$; two-tailed unpaired Student's *t*-test (**a, e**) or two-way ANOVA (**b, c, f**). Data are from three (**a, b, e**) or two (**c, d, f**) independent experiments

under steady state. The frequencies and numbers of Tregs in LKB1$^{\Delta DC}$ mice were increased in all tissues examined (Fig. 2a). To exclude the possibility of CD11c-Cre-mediated gene deletion in Tregs, we examined *Stk11* expression in Tregs and found minimal *Stk11* deletion in Tregs of LKB1$^{\Delta DC}$ mice (Supplementary information, Fig. S2a). To determine the cell-intrinsic effect of LKB1 in DCs on Treg homeostasis, we generated mixed bone marrow chimeras by reconstituting lethally irradiated CD45.1$^+$ mice with bone marrow cells from CD45.1.2$^+$ mice (spike), together with cells from WT or LKB1$^{\Delta DC}$ mice (CD45.2.2$^+$ donor) at a 1:1 ratio. The frequency and number of Tregs derived from the LKB1-deficient donors were higher than those of the WT counterparts (Supplementary information, Fig. S2b). Furthermore, spike cells in the chimeras transferred with bone marrow cells from LKB1$^{\Delta DC}$ mice also exhibited higher Treg frequency and number compared with those in WT chimeras (Supplementary information, Fig. S2b), indicating the dominant effect of LKB1 deficiency in DCs on Treg homeostasis. Therefore, LKB1 deficiency in DCs promotes Treg generation in a cell-intrinsic and dominant manner.

Tregs can be divided into tTregs and pTregs based on their location of induction.[8] Compared with pTregs, tTregs express higher levels of neuropilin-1 (Nrp1) and Helios,[26–28] although Helios can be induced in peripherally induced pTregs under selective contexts.[29] The majority of increased Tregs in the spleen of LKB1$^{\Delta DC}$ mice were Nrp1$^+$ (Fig. 2b) and Helios$^+$ tTregs (Supplementary information, Fig. S2c), except for a small increase in Helios$^-$ Tregs in the spleen. We next examined pTreg and tTreg populations in the colon lamina propria of LKB1$^{\Delta DC}$ mice by staining for either Helios or RORγt, a transcription factor selectively enriched in pTregs from the intestines.[30,31] Similar to our findings in the spleen, Helios$^+$ or RORγt$^-$ tTregs were increased in the colon lamina propria of LKB1$^{\Delta DC}$ mice, while pTregs were similar (Fig. 2c; Supplementary information, Fig. S2d). We next used two approaches to conclusively test the effects of LKB1-deficient DCs on pTreg induction. First, we used a model of oral antigen-induced Treg generation by transferring naïve CD4$^+$ T cells from OT-II mice, which have transgenic expression of a TCR specific for ovalbumin (OVA) amino acids 323–339 (OVA$_{323–339}$), into WT and LKB1$^{\Delta DC}$ mice, followed by feeding the mice with OVA protein in the drinking water.[32,33] Donor cells developed into comparable Foxp3$^+$ population in the spleen, mesenteric lymph nodes (MLN) and Peyer's patches from WT and LKB1$^{\Delta DC}$ mice (Fig. 2d). Second, we co-cultured naïve OT-II CD4$^+$ T cells with WT and LKB1-deficient DCs from MLN in the presence of OVA$_{323–339}$, without exogenous cytokines. Five days later, CD4$^+$ T cells cultured with LKB1-deficient DCs developed into a lower frequency of Foxp3$^+$ T cells (Fig. 2e). Similarly, splenic DCs from LKB1$^{\Delta DC}$ mice showed a modestly reduced ability to induce Foxp3 expression from naïve T cells (Supplementary information, Fig. S2e). Thus, LKB1-deficient DCs preferentially promote accumulation of tTregs but not pTregs.

Moreover, Treg activation-associated molecules CD103, ICOS, CTLA-4 and CD44 were expressed at higher levels, whereas CD62L and CD25 were expressed at lower levels on Tregs from LKB1$^{\Delta DC}$ mice (Fig. 2f). Further analysis revealed that both CD25$^+$ and CD25$^-$ subsets of Tregs were increased in LKB1$^{\Delta DC}$ mice, with a more pronounced increase of the CD25$^-$ Treg subset (Supplementary information, Fig. S2f). The in vitro suppressive activity of Tregs from LKB1$^{\Delta DC}$ mice was also enhanced (Fig. 2g). Thus, loss of LKB1 in DCs preferentially promotes tTreg accumulation and their functional activation.

LKB1 functions in DCs to restrain Treg peripheral proliferation and thymic development

To determine the underlying mechanisms for the increased Tregs in LKB1$^{\Delta DC}$ mice, we examined Treg apoptosis and proliferation by active caspase-3 staining and 5-bromodeoxyuridine (BrdU) incorporation assays, respectively. Compared with WT counterparts,

Tregs from LKB1$^{\Delta DC}$ mice had comparable active caspase-3 staining (Supplementary information, Fig. S3a), but more BrdU incorporation (Fig. 3a). The staining of Ki-67, a molecular marker for cell proliferation, also revealed the increased proliferation of Tregs from LKB1$^{\Delta DC}$ mice (Supplementary information, Fig. S3b). Consistent with the expansion of the Treg pool in LKB1$^{\Delta DC}$ mice, the increase in Treg frequency occurred in the spleen of neonatal mice and positively correlated with the mouse age (Supplementary information, Fig. S3c). We then examined the direct effects of LKB1 signaling in DCs on Treg proliferation using in vivo and in vitro systems. In the in vivo system, we labeled WT CD45.1$^+$ Tregs with CellTrace Violet (CellTrace), transferred them into WT and LKB1$^{\Delta DC}$ mice, and assessed CellTrace dilution seven days later. The frequency of CellTrace^{lo} Tregs in LKB1$^{\Delta DC}$ mice was significantly higher than those from WT mice (Fig. 3b). In vitro, WT Tregs were cultured with WT or LKB1-deficient splenic DCs, and thymidine incorporation analysis showed that LKB1-deficient DCs exhibited an enhanced ability to promote Treg proliferation (Fig. 3c). Altogether, LKB1 deficiency in DCs promotes peripheral Treg proliferation.

To identify the mechanisms underlying the increased Treg proliferation, we compared gene expression profiles of Tregs isolated from WT and LKB1$^{\Delta DC}$ mice using gene-set enrichment analysis (GSEA). Tregs exhibit elevated steady state mTOR activity compared with naïve T cells, which programs their generation and function.[34,35] GSEA showed that Tregs from LKB1$^{\Delta DC}$ mice upregulated mTORC1 signaling and several metabolic pathways, including glycolysis, cholesterol homeostasis and fatty acid metabolism (Supplementary information, Fig. S3d). Consistent with this analysis, we found that Tregs from LKB1$^{\Delta DC}$ mice had increased expression of phosphorylated S6 than WT Tregs in spleen and PLN (Fig. 3d), suggesting that LKB1-deficient DCs activate mTORC1 signaling in Tregs. IL-2 also plays an important role in controlling the survival and function of Tregs.[36] DCs have been shown to produce IL-2,[37] and we found that LKB1-deficient DCs had increased IL-2 expression at both mRNA and protein levels compared with WT DCs (Fig. 3e; Supplementary information, Fig. S3e). Furthermore, there was increased IL-2 expression in both CD4 and CD8 T cells in LKB1$^{\Delta DC}$ mice (Supplementary information, Fig. S3f). To verify the effect of IL-2 on Treg proliferation, we pretreated WT and LKB1$^{\Delta DC}$ mice with anti-IL-2 antibodies, and then transferred CellTrace-labelled WT Tregs into them. Anti-IL-2 antibody blockade abrogated increased Treg proliferation in LKB1$^{\Delta DC}$ mice (Supplementary information, Fig. S3g). Similarly, when IL-2 signaling was blocked in the in vitro co-culture system, the proliferation of Tregs was decreased (Fig. 3f). Aside from IL-2, other γc cytokines IL-7 and IL-15 can also promote Treg expansion and development.[38] Accordingly, *Il7* and *Il15* mRNA levels were also elevated in LKB1-deficient DCs (Fig. 3e), although IL-7 secretion amount was below detectable level and IL-15 secretion was also low and did not differ significantly between WT and LKB1-deficient DCs (Supplementary information, Fig. S3e). Furthermore, blocking antibodies for IL-7 or IL-15 had no effect on Treg proliferation induced by either WT or LKB1-deficient DCs (Supplementary information, Fig. S3h). Collectively, these results suggest that LKB1 functions in DCs to limit peripheral Treg proliferation, with IL-2 playing a role in this process.

We next determined the processes underlying the increased Tregs in the thymus of LKB1$^{\Delta DC}$ mice, which can result from enhanced Treg proliferation and/or generation. Efficient deletion of *Stk11* was found in thymic DCs from LKB1$^{\Delta DC}$ mice (Supplementary information, Fig. S3i). In line with our ex vivo data showing increased thymic Treg proliferation from LKB1$^{\Delta DC}$ mice described above, LKB1-deficient thymic DCs had an enhanced ability to promote proliferation of thymic Tregs in vitro as compared with WT cells (Fig. 3g), similar as the observations from splenic DCs. In addition, Foxp3$^+$ Tregs can be induced from tTreg precursors by thymic DCs.[39] We therefore co-cultured thymic DCs
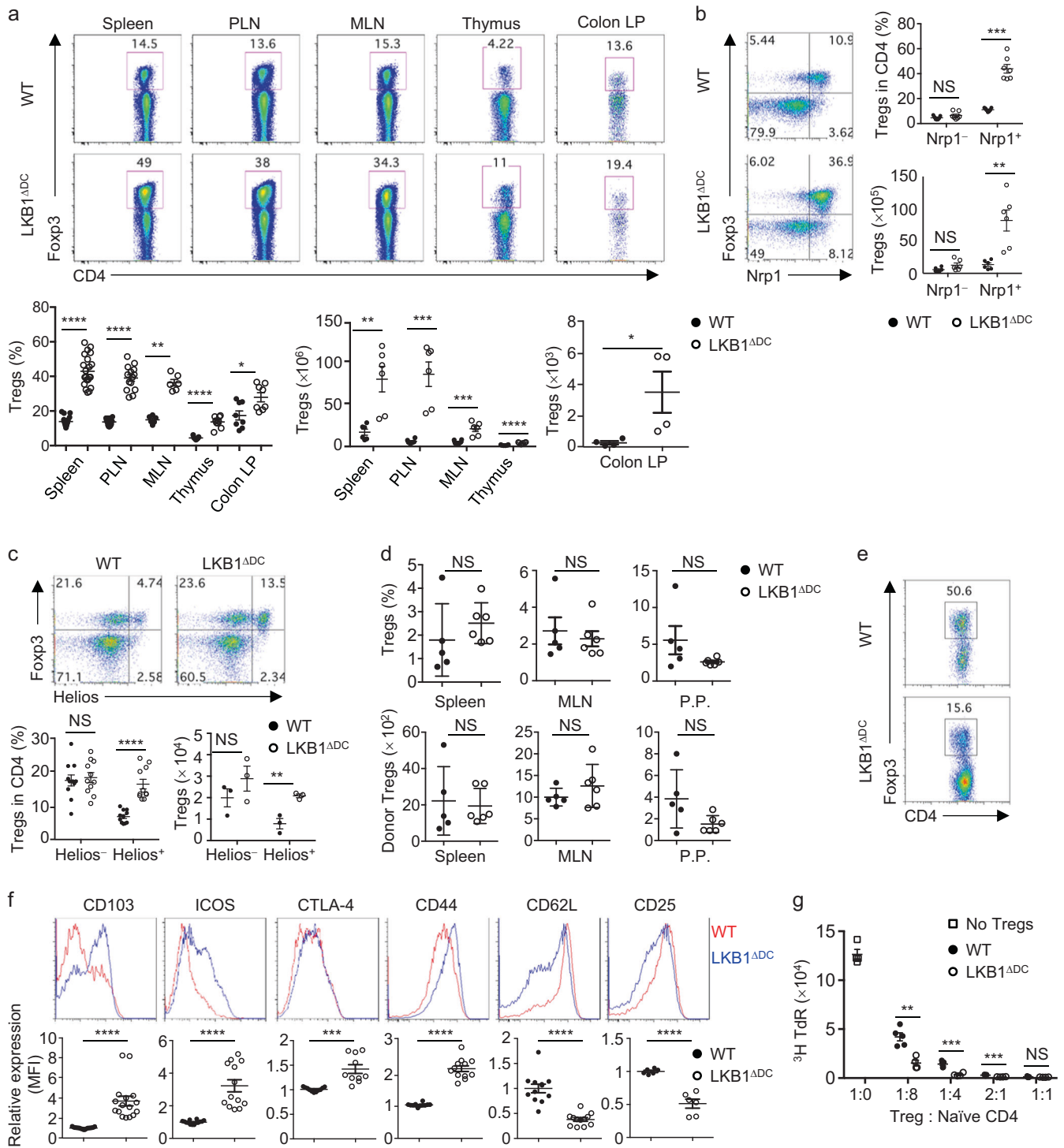
Fig. 2 LKB1 deficiency in DCs results in increased tTreg accumulation. **a** Flow cytometry analysis (upper) and frequencies (lower) of Foxp3+CD4+ Tregs in the spleen, peripheral lymph nodes (PLN), mesenteric lymph nodes (MLN), thymus and colon lamina propria (LP) of WT and LKB1$^{\Delta DC}$ mice. **b** Flow cytometry analysis of Foxp3 and neuropilin-1 (Nrp1) expression (left) and statistics of frequencies and numbers of Nrp1$^-$ and Npr1$^+$ Tregs among CD4+TCRβ+ T cells (right) in the spleen of WT and LKB1$^{\Delta DC}$ mice. **c** Flow cytometry analysis of Foxp3 and Helios expression (upper) and statistics of frequencies and numbers of Helios$^-$ and Helios$^+$ Tregs among CD4+TCRβ+ T cells (lower) in the colon LP of WT and LKB1$^{\Delta DC}$ mice. **d** After adoptive transfer of naïve OT-II CD4+ T cells, WT and LKB1$^{\Delta DC}$ mice were fed with water supplemented with OVA protein. Five days later, the cells from spleen, MLN and Peyer's patches (P.P.) were examined for the frequencies and numbers of Foxp3$^+$ cells among donor cells. **e** Flow cytometry analysis of Foxp3 expression in naïve OT-II CD4+ T cells cultured with CD103+ MLN DCs from WT and LKB1$^{\Delta DC}$ mice for 5 days. **f** Flow cytometry analysis (upper) and statistics of relative mean fluorescence intensity (MFI, lower) of CD103, ICOS, CTLA-4, CD44, CD62L and CD25 expression in splenic Tregs from WT and LKB1$^{\Delta DC}$ mice. The MFI in WT Tregs was set as 1. **g** In vitro suppressive activity of Tregs isolated from WT and LKB1$^{\Delta DC}$ mice. Data in plots indicate the means ± s.e.m; each symbol represents an individual mouse. Numbers in quadrants or gates indicate percentage of cells. *NS* not significant; *P < 0.05, **P < 0.01, ***P < 0.001, ****P < 0.0001; two-tailed Mann-Whitney test (**a**–**d**, frequency) or two-tailed unpaired Student's t-test (**a**–**d**, cell number; **f**, **g**). Data are from at least three (**a**, **b**, **f**) or two (**c**–**e**, **g**) independent experiments
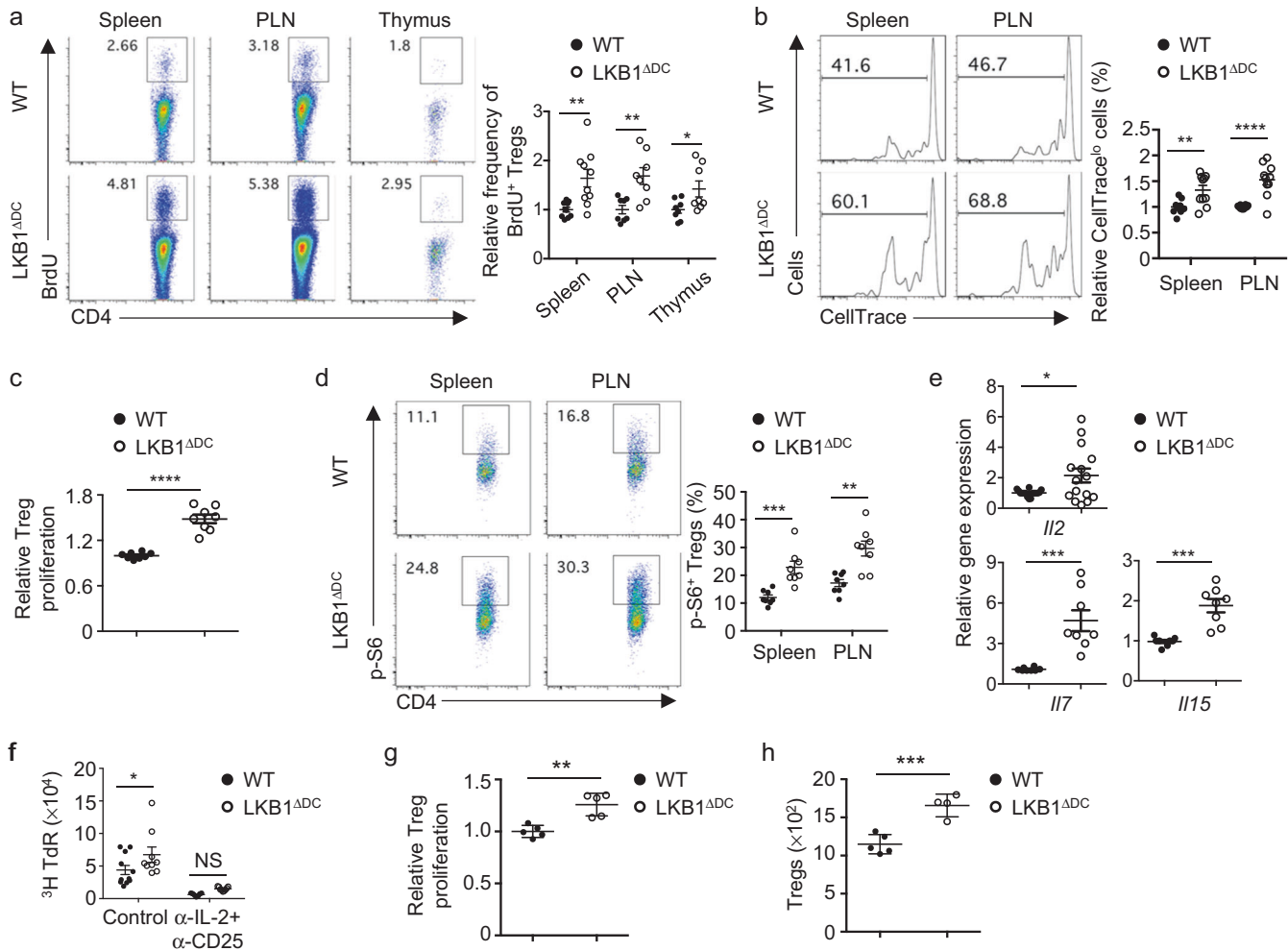
Fig. 3 LKB1 functions in DCs to restrain excessive Treg expansion and thymic differentiation. **a** Flow cytometry analysis (left) and statistics (right) of BrdU incorporation in CD4$^+$TCRβ$^+$Foxp3$^+$ Tregs in the spleen, PLN and thymus of WT and LKB1$^{\Delta DC}$ mice. **b** CellTrace-labelled CD45.1$^+$ Tregs were transferred into WT and LKB1$^{\Delta DC}$ mice and the CellTrace dilution was analyzed seven days later (left). Right, the relative percentage of CellTrace^{lo} cells. The percentage of CellTrace^{lo} cells in WT mice was set as 1. **c** Relative thymidine incorporation of WT Tregs cultured with splenic DCs from WT and LKB1$^{\Delta DC}$ mice (values cultured with WT splenic DCs was set as 1). **d** Flow cytometry analysis (left) and statistics (right) of p-S6 expression in CD4$^+$TCRβ$^+$Foxp3$^+$ Tregs in the spleen and PLN of WT and LKB1$^{\Delta DC}$ mice. **e** Real-time PCR analysis of *Il2, Il7* and *Il15* mRNA expression in untreated splenic DCs from WT and LKB1$^{\Delta DC}$ mice. **f** Thymidine incorporation of WT Tregs cultured with splenic DCs from WT and LKB1$^{\Delta DC}$ mice in the presence or absence of anti-IL-2 + anti-CD25 blocking antibodies. **g** Relative thymidine incorporation of WT thymic Tregs cultured with thymic DCs from WT and LKB1$^{\Delta DC}$ mice (values cultured with WT thymic DCs was set as 1). **h** CD4$^+$CD8$^-$CD25$^-$YFP-Foxp3$^-$ thymocytes (tTreg precursors) were cultured with thymic DCs from WT and LKB1$^{\Delta DC}$ mice in the presence of 10 ng/mL IL-7 for 4 days and analyzed for Foxp3$^+$ Treg induction. Data in plots indicate the means ± s.e.m; each symbol represents an individual mouse. Numbers in gates indicate percentage of cells. *NS* not significant; *$P < 0.05$, **$P < 0.01$, ***$P < 0.001$, ****$P < 0.0001$; two-tailed Mann–Whitney test (**a**, **b**, **d**) or two-tailed unpaired Student's *t*-test (**c**, **e**–**h**). Data are from at least three (**a**–**f**) or two (**g**, **h**) independent experiments

with CD4$^+$CD8$^-$CD25$^-$Foxp3$^-$ thymocytes (tTreg precursors in the thymus) by following the published procedure,[39] and found that LKB1-deficient thymic DCs induced more Tregs (Fig. 3h). Further analysis showed that the number and frequency of total thymic DCs were comparable between WT and LKB1$^{\Delta DC}$ mice (Supplementary information, Fig. S3j). However, compared with WT controls, LKB1$^{\Delta DC}$ mice had an increased frequency and number of CD11b$^+$ thymic DCs (Supplementary information, Fig. S3j), which have been reported to have superior capacity to induce de novo Treg generation from tTreg precursors.[39] Thus, LKB1 deficiency in thymic DCs promotes tTreg proliferation and generation.

LKB1 deficiency in DCs promotes Th17 cell differentiation
From tumor tissue analysis, we found increased IL-17 production by T cells from tumor-infiltrating lymphocytes and draining lymph nodes of LKB1$^{\Delta DC}$ mice (Fig. 4a). Th17-associated cytokines have

been shown to have both anti-tumorigenic and pro-tumorigenic functions dependent upon the specific context.[40] We therefore tested the contribution of IL-17 to increased MC38 tumor growth in LKB1$^{\Delta DC}$ mice by generating LKB1$^{\Delta DC}$ mice that also lacked IL-17Rα. We challenged LKB1$^{\Delta DC}$*Il17ra*$^{-/-}$ mice with MC38 tumor cells, and found that IL-17Rα deficiency partially decreased tumor growth as compared to LKB1$^{\Delta DC}$ mice (Fig. 4b), indicating a tumor-promoting role of IL-17 signaling in this context.

Under steady state, CD44^{hi} CD4$^+$ and CD8$^+$ T cells in spleen of LKB1$^{\Delta DC}$ mice expressed significantly higher levels of IL-17, and CD44^{hi} CD8$^+$ T cells also had modestly higher IFN-γ (Fig. 4c). We first confirmed that the increased IL-17 expression did not result from aberrant deletion of *Stk11* in Th17 (CD4$^+$CD44^{hi}CCR6$^+$) cells from LKB1$^{\Delta DC}$ mice (Supplementary information, Fig. S4a). We then used both in vivo and in vitro methods to examine the requirement of LKB1 in DCs in Th17 cell responses. First, WT and
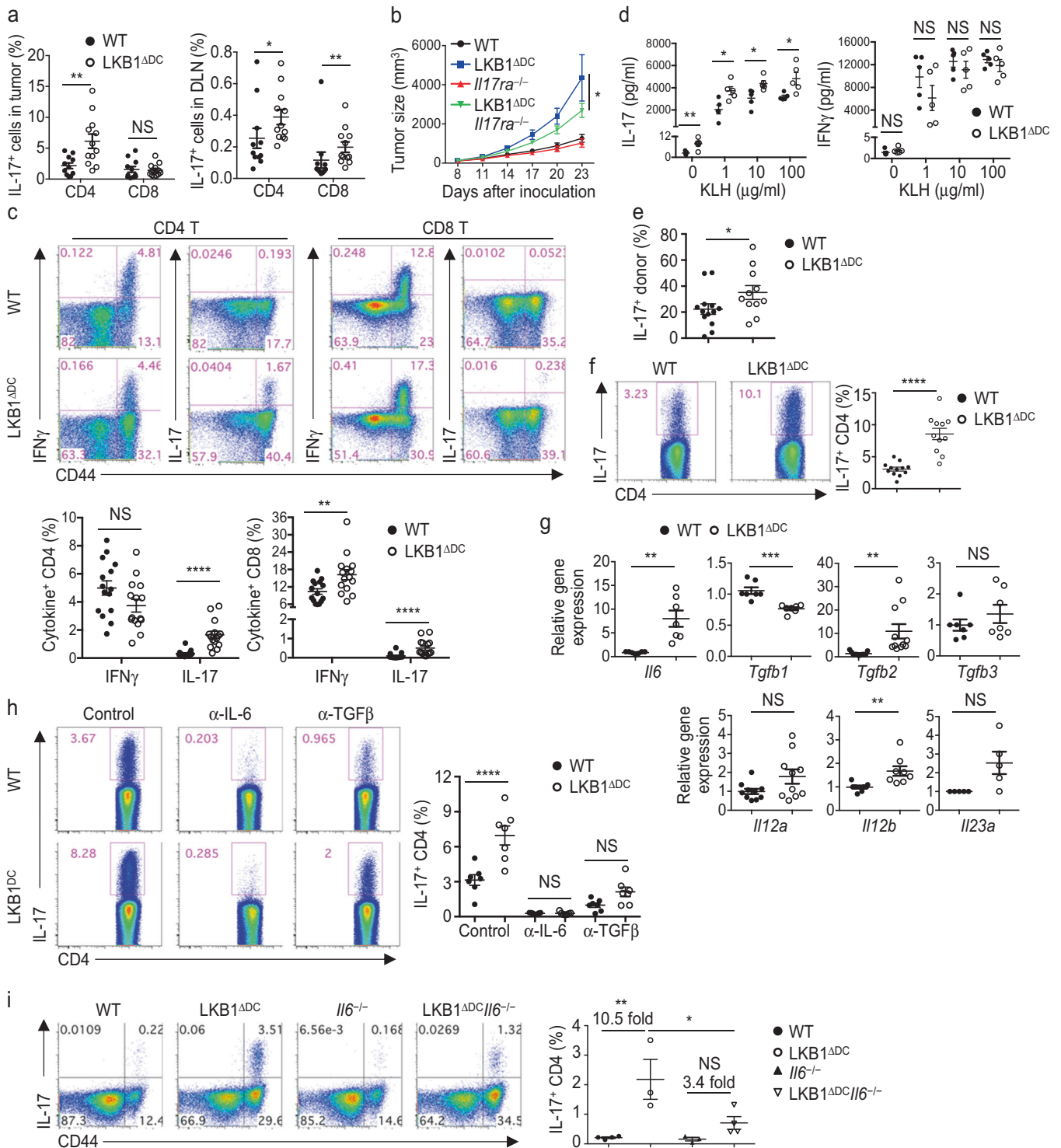
LKB1$^{\Delta DC}$ mice were immunized in their footpad with keyhole limpet hemocyanin (KLH) emulsified with complete Freund's adjuvant (CFA), and 7 days later, draining lymph node cells were isolated and restimulated with different doses of KLH for the recall responses. T cells from LKB1$^{\Delta DC}$ mice produced higher levels of IL-17, but not IFNγ, compared with their WT controls (Fig. 4d). Real-time PCR analysis also demonstrated increased *Il17* mRNA expression in T cells from LKB1$^{\Delta DC}$ mice after KLH immunization (Supplementary information, Fig. S4b). Second, to directly analyze the role of DC LKB1 signaling in de novo Th17 cell differentiation,

we transferred naïve OT-II CD4$^+$ T cells into WT or LKB1$^{\Delta DC}$ mice, followed by footpad immunization with OVA$_{323–336}$ in CFA. Donor CD4$^+$ T cells isolated from the draining lymph nodes of LKB1$^{\Delta DC}$ mice expressed higher levels of IL-17 compared to those from WT mice (Fig. 4e). Third, naïve OT-II CD4$^+$ T cells co-cultured with LKB1-deficient splenic DCs in the presence of OVA$_{323–336}$ in vitro produced higher levels of IL-17 (Fig. 4f). Altogether, these results indicate that LKB1-deficient DCs promote Th17 cell differentiation.

We next dissected the cellular mechanisms by which LKB1 regulated DC-mediated Th17 cell differentiation. We examined the

Fig. 4 LKB1 deficiency in DCs promotes Th17 cell differentiation in an IL-6-dependent manner. **a** Statistics of IL-17 expression in CD4$^+$ and CD8$^+$ T cells in tumor-infiltrating lymphocytes and tumor draining lymph nodes (DLN) of WT and LKB1$^{\Delta DC}$ mice. **b** Tumor growth curve in WT ($n = 16$), LKB1$^{\Delta DC}$ ($n = 8$), Il17ra$^{-/-}$ ($n = 10$) and LKB1$^{\Delta DC}$Il17ra$^{-/-}$ ($n = 13$) mice following inoculation of MC38 tumor cells. **c** Flow cytometry analysis (upper) and statistics (lower) of IFNγ and IL-17 expression in splenic CD4$^+$ and CD8$^+$ T cells from WT and LKB1$^{\Delta DC}$ mice. **d** Analysis of IL-17 and IFN-γ levels in the culture supernatant of popliteal DLN cells from KLH immunized WT and LKB1$^{\Delta DC}$ mice after ex vivo stimulation with KLH for 72 h. **e** WT and LKB1$^{\Delta DC}$ mice were transferred with naïve OT-II CD4$^+$ T cells, followed by footpad immunization with OVA/CFA. IL-17 expression in donor-derived CD4$^+$ T cells in the popliteal DLN was analyzed seven days later. **f** Flow cytometry analysis (left) and statistics (right) of IL-17 expression in naïve OT-II CD4$^+$ T cells cultured with splenic DCs from WT and LKB1$^{\Delta DC}$ mice for 5 days. **g** Real-time PCR analysis of Il6, Tgfb1, Tgfb2, Tgfb3, Il12a, Il12b, and IL23a mRNA expression in untreated splenic DCs from WT and LKB1$^{\Delta DC}$ mice. **h** Flow cytometry analysis (left) and statistics (right) of IL-17 expression in naïve OT-II CD4$^+$ T cells cultured with splenic DCs from WT and LKB1$^{\Delta DC}$ mice for 5 days in the presence or absence of anti-IL-6 or anti-TGFβ blocking antibodies. **i** Flow cytometry analysis (left) and statistics (right) of IL-17 expression in splenic CD4$^+$ T cells from WT, LKB1$^{\Delta DC}$, Il6$^{-/-}$, or LKB1$^{\Delta DC}$Il6$^{-/-}$ mice. Numbers in the statistics graph indicate fold changes of IL-17 expression in LKB1$^{\Delta DC}$ vs WT mice, and LKB1$^{\Delta DC}$Il6$^{-/-}$ vs Il6$^{-/-}$ mice, respectively. Data in plots indicate the means ± s.e.m; each symbol represents an individual mouse. Numbers in quadrants or gates indicate percentage of cells. NS not significant; *$P < 0.05$, **$P < 0.01$, ***$P < 0.001$, ****$P < 0.0001$; two-tailed Mann–Whitney test (**a**, **c**, **e**, **f**, **h**), two-tailed unpaired Student's t-test (**d**, **g**), or two-way ANOVA (**b**, **i**). Data are from at least three (**a**, **c**, **e**–**g**, **i**) or two (**b**, **d**, **h**) independent experiments

expression of cytokines known to regulate Th17 cell differentiation.[41] The mRNA expression of IL-6 and TGFβ2 were drastically increased in LKB1-deficient DCs from the spleen compared to WT DCs (Fig. 4g), which were found in both the LKB1-deficient CD8α$^+$ and CD8α$^-$ cDC subsets (Supplementary information, Fig. S4c). In contrast, TGFβ1 and TGFβ3 were modestly decreased or showed no difference (Fig. 4g). Additionally, IL-12 p40 mRNA expression was slightly increased in LKB1-deficient DCs, whereas IL-12 p35 and IL-23 p19 mRNAs were normal (Fig. 4g). We further measured IL-6, TGFβ1, TGFβ2, and TGFβ3 levels in the supernatant from Th17 cell differentiation cultures and found that the production of IL-6, and to a lesser extent, TGFβ2, was significantly increased in the supernatant of LKB1-deficient DC and T cell co-cultures, while the production of TGFβ1 and TGFβ3 was comparable to that of WT controls (Supplementary information, Fig. S4d). To ascertain whether increased IL-6 and TGFβ2 account for the increased differentiation of Th17 cells, we blocked IL-6 and TGFβ in the in vitro co-culture system. Anti-IL-6 antibodies substantially blocked the increased expression of IL-17 in CD4$^+$ T cells induced by LKB1-deficient DCs (Fig. 4h). In contrast, anti-TGFβ antibodies showed only a partial effect on blocking the increased Th17 differentiation (Fig. 4h), and did not affect Treg proliferation (Supplementary information, Fig. S4e), suggesting a more crucial involvement of IL-6 downstream of LKB1 deletion in driving aberrant Th17 cell differentiation. We therefore used a genetic model to further explore the role of IL-6 in IL-17 production. Deletion of IL-6 substantially, though incompletely, inhibited the ability of LKB1-deficient DCs to promote IL-17 expression by CD4$^+$ T cells (Fig. 4i), but it had no effect on the accumulation of Tregs (Supplementary information, Fig. S4f). In addition, IL-17 production by naïve OT-II CD4$^+$ T cells, when co-cultured with DCs deficient for both LKB1 and IL-6, was also decreased and comparable to that in OT-II CD4$^+$ T cells co-cultured with WT DCs (Supplementary information, Fig. S4g). Furthermore, when challenged with MC38 tumor cells, LKB1$^{\Delta DC}$Il6$^{-/-}$ mice had largely suppressed tumor growth compared with LKB1$^{\Delta DC}$ mice (Supplementary information, Fig. S4h). IL-17 has been shown to mediate protective immunity[42,43] or promote tumor development partially through activating IL-6−STAT3 pathway.[44] We found that LKB1$^{\Delta DC}$ mice treated with the STAT3 inhibitor showed partially inhibited tumor growth (Supplementary information, Fig. S4i). Taken together, LKB1 signaling in DCs is crucial for the control of tumor-promoting Th17 cell differentiation, in part by shaping IL-6 −STAT3 signaling.

LKB1 enforces immune and metabolic quiescence in DCs
To explore the cellular and molecular pathways mediated by LKB1, we examined the effects of LKB1 deficiency on DC homeostasis and function. Flow cytometry analysis of DC maturation markers showed normal expression of CD80, but increased expression of CD86, CD40 and MHC-II on LKB1-deficient splenic DCs (Fig. 5a). In addition, LKB1-deficient thymic DCs also had increased expression of CD86 and to a lesser extent, MHC-II (Supplementary information, Fig. S5a). Moreover, mixed bone marrow chimera experiments demonstrated a cell-intrinsic role of LKB1 in controlling DC maturation marker expression (Supplementary information, Fig. S5b). The proliferation and apoptosis assays showed slightly but significantly increased BrdU incorporation, and largely normal apoptosis of LKB1-deficient DCs (Supplementary information, Fig. S5c, d). Aside from γc homeostatic cytokines, DCs produce other cytokines or molecules to promote Treg generation, including Arg2, Ido1, and integrin β8.[45–47] We found increased expression of Arg2, Ido1 and Itgb8 in LKB1-deficient DCs (Fig. 5b). Based on the phenotypes and origins, DCs can be classified into lymphoid-resident DCs and migratory DCs,[1] and migratory DCs have been reported to promote tTreg accumulation.[48] We found a significantly increased frequency of migratory DCs in the PLN from LKB1$^{\Delta DC}$ mice (Supplementary information, Fig. S5e). Flow cytometry analysis also showed that LKB1-deficient DCs had increased expression of CCR7 (Supplementary information, Fig. S5f), which can regulate DC migration to lymph nodes.[49] CD86 and CD80 on DCs can interact with CD28 expressed on Tregs to mediate Treg homeostasis.[50] Immunofluorescence analysis showed that there was increased DC-Treg interaction in the PLN of LKB1$^{\Delta DC}$ mice (Fig. 5c). Collectively, LKB1 deficiency promotes DC maturation, expression of immunoregulatory molecules, and DC-Treg interaction.

To comprehensively dissect the mechanisms by which LKB1 regulates DC function, we performed transcriptomics and proteomics profiling of WT and LKB1-deficient DCs. GSEA of both gene expression and proteome profiling indicated that LKB1-deficient DCs had upregulated the hallmark cholesterol homeostasis pathway (Fig. 6a, b). We also found Dhcr24, encoding 3β-hydroxysterol Δ24-reductase, the final enzyme of the cholesterol biosynthetic pathway, was increased in LKB1-deficient DCs (Fig. 6c). The expression of Abca1, Abcg1, and Abcg3, encoding ATP-binding cassette (ABC) transporter A1 (ABCA1), ABCG1 and ABCG3, respectively, which mediate cholesterol efflux from immune cells, was decreased in LKB1-deficient DCs (Fig. 6d). Consistent with these findings, flow cytometry analysis of BODIPY staining revealed increased accumulation of lipids in LKB1-deficient DCs (Fig. 6e). Since cholesterol-enriched DCs produce increased proinflammatory cytokines and promote T cell activation,[51] the altered cholesterol metabolism is likely one of the mechanisms utilized by LKB1 in DCs to control T cell homeostasis. We further measured the oxygen consumption rate (OCR, an indicator of oxidative phosphorylation) and extracellular acidification rate (ECAR, an indicator of glycolysis) of WT and LKB1-deficient DCs, and found LKB1-deficient DCs showed higher OCR and ECAR than WT DCs (Fig. 6f). Moreover, LKB1-deficient DCs had
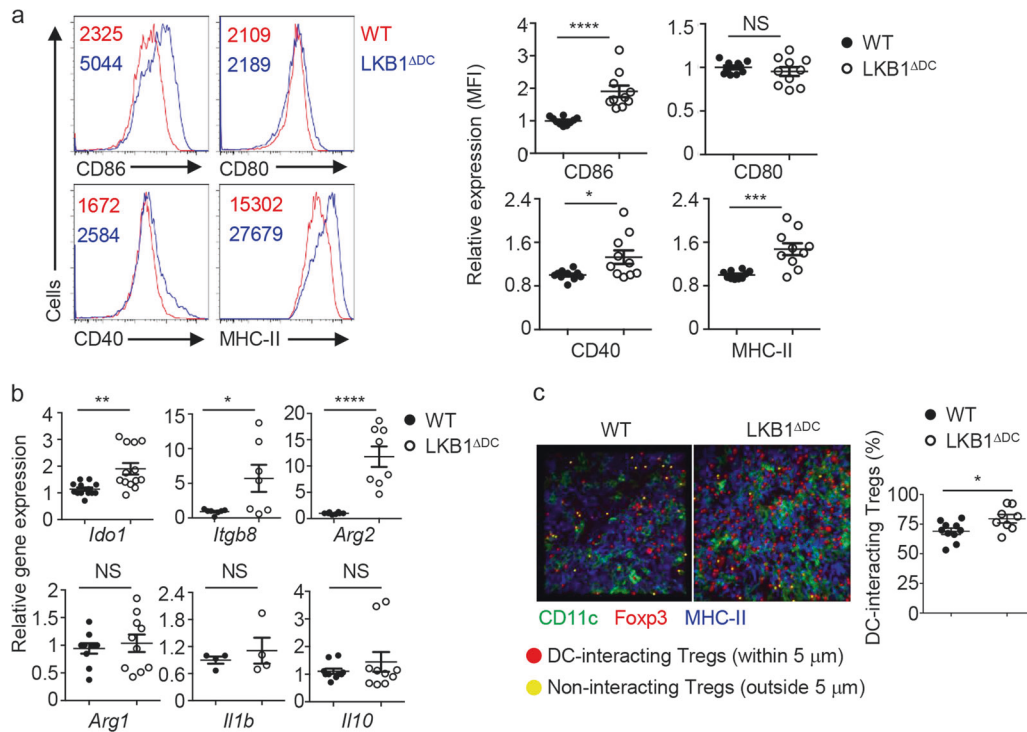
Fig. 5 LKB1 deficiency promotes DC maturation, expression of immunoregulatory molecules, and DC-Treg interaction. **a** Flow cytometry analysis (left) and statistics (right) of CD86, CD80, CD40 and MHC-II expression on splenic DCs from WT and LKB1$^{\Delta DC}$ mice. The mean fluorescence intensity (MFI) in WT DCs was set as 1. Each symbol represents an individual mouse. **b** Real-time PCR analysis of gene expression in splenic cDCs from WT and LKB1$^{\Delta DC}$ mice. Each symbol represents an individual mouse. **c** Representative immunofluorescence images (left) and statistics of DC-interacting Treg percentage in PLN (right) of WT and LKB1$^{\Delta DC}$ mice. Each symbol represents an individual field. Data in plots indicate the means ± s.e.m. Numbers in graphs indicate the mean fluorescence intensity (MFI). *NS* not significant; *$P < 0.05$, **$P < 0.01$, ***$P < 0.001$, ****$P < 0.0001$; two-tailed unpaired Student's *t*-test (**a–c**). Data are from four (**a**), at least two (**b**), or three (**c**) independent experiments

increased cell size (Fig. 6g). Altogether, LKB1 deficiency upregulates DC activation molecules and metabolic profiles, suggesting that LKB1 coordinates immune and metabolic quiescence in DCs.

LKB1 maintains DC quiescence partially through restricting mTOR signaling
AMPK is a well-documented substrate of LKB1 and exists as two isoforms: AMPKα1 and AMPKα2 (encoded by *Prkaa1* and *Prkaa2*, respectively).[15] To determine the functional relevance of AMPK signaling, we crossed mice carrying floxed *Prkaa1* and *Prkaa2* alleles with CD11c-Cre mice and generated AMPK1/2$^{\Delta DC}$ mice to eliminate all AMPK activity in DCs. To our surprise, the frequencies of cDCs, pDCs, and CD8α$^+$ and CD8α$^-$ subsets were comparable in WT and AMPK1/2$^{\Delta DC}$ mice (Supplementary information, Fig. S6a), with normal expression of CD86, CD80, CD40 and MHC-II on AMPK1/2-deficient DCs (Supplementary information, Fig. S6b). In addition, AMPK1/2$^{\Delta DC}$ mice had normal proportion of total Tregs (Supplementary information, Fig. S6c), and undisturbed cytokine expression of conventional T cells (Supplementary information, Fig. S6d). Moreover, previous studies showed that HIF-1α is an important effector pathway in LKB1-deficient cancer cells.[52] Unexpectedly, in LKB1/HIF-1α$^{\Delta DC}$ mice, depletion of HIF-1α in LKB1-deficient DCs failed to rescue the aberrant DC maturation and excessive Treg and Th17 responses (Supplementary information, Fig. S6e, f). Thus, LKB1 signaling in DCs functions independently of the conventional AMPK and HIF-1α pathways to control DC and T cell homeostasis.

GSEA of gene expression and whole proteome profiling of WT and LKB1-deficient DCs revealed increased mTORC1 signaling in LKB1-deficient DCs (Fig. 6b, Fig. 7a). Immunoblot and phospho-flow analyses verified that LKB1-deficient DCs had increased

mTORC1 targets, i.e., phosphorylation of S6 and 4E-BP1 (Fig. 7b; Supplementary information, Fig. S6g). In addition, phosphorylated AKT (Ser473), an indicator of mTORC2 activity, was increased in LKB1-deficient DCs (Fig. 7b). To determine the contribution of increased mTOR activity to the phenotypes observed above, we crossed LKB1$^{\Delta DC}$ mice with those carrying floxed *Mtor* alleles (*Mtor*$^{fl/fl}$) and generated LKB1/mTOR$^{\Delta DC}$ mice. Compared with LKB1-deficient DCs, DCs from LKB1/mTOR$^{\Delta DC}$ mice had decreased expression of CD86, CD40 and MHC-II (Fig. 7c), but similar levels of *Il2*, *Il7* and *Il15* (Supplementary information, Fig. S6h). The frequencies of total Tregs, CD103$^+$ Tregs and Ki-67$^+$ Tregs in LKB1/mTOR$^{\Delta DC}$ mice were significantly decreased compared with LKB1$^{\Delta DC}$ mice (Fig. 7d, e). The percentage of p-S6$^+$ Tregs was also decreased in LKB1/mTOR$^{\Delta DC}$ mice compared with those in LKB1$^{\Delta DC}$ mice (Fig. 7f). However, mTOR deficiency in DCs had no rescue effect on the increased IL-17 expression by CD4$^+$ and CD8$^+$ T cells (Fig. 7g; Supplementary information, Fig. S6i). Collectively, our results show that LKB1 acts in a partially mTOR-dependent manner to maintain DC quiescence and DC-mediated control of Tregs.

DISCUSSION
The inhibitory pathways that restrict DC-mediated effector and regulatory T cell responses are less understood. Similarly, despite the recent emphasis on the pathways that activate metabolic reprogramming of DCs,[10,11] how DC metabolism is negatively regulated remains poorly defined. Here we have identified that LKB1 signaling is critical to restrict excessive Treg expansion and Th17 cell differentiation by establishing metabolic quiescence in DCs. Although differentiation of induced Treg cells and Th17 cells
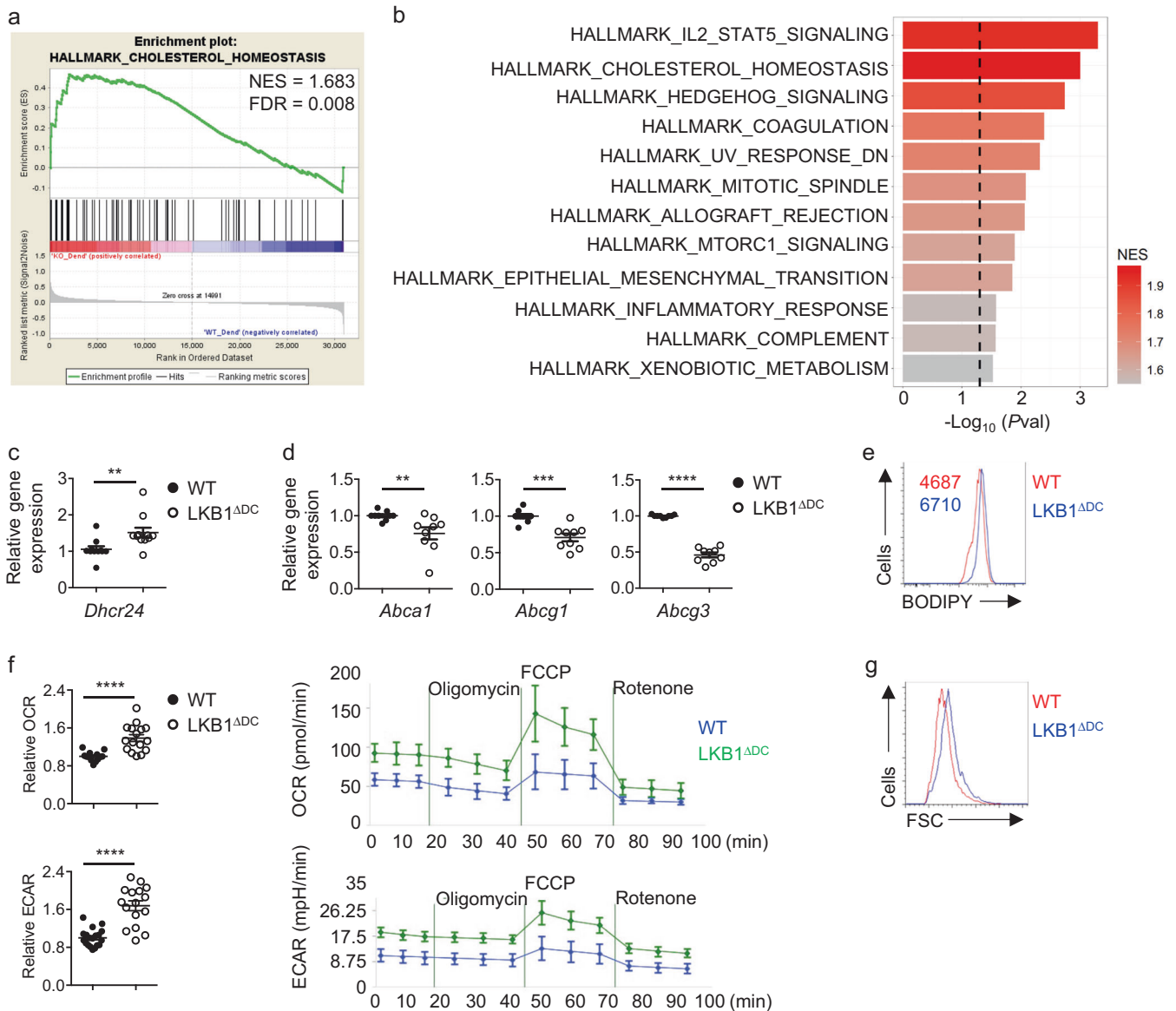
Fig. 6 LKB1 deficiency in DCs results in loss of metabolic quiescence. **a** Enrichment plot of the hallmark cholesterol homeostasis in LKB1-deficient splenic DCs compared to WT DCs profiled using gene expression, identified by gene set enrichment analysis (GSEA). **b** GSEA identified top 10 hallmark pathways enriched in LKB1-deficient splenic DCs compared to WT DCs profiled using proteomics. **c** Real-time PCR analysis of *Dhcr24* mRNA expression in splenic cDCs from WT and LKB1$^{\Delta DC}$ mice. Each symbol represents an individual mouse. **d** Real-time PCR analysis of *Abca1*, *Abcg1* and *Abcg3* mRNA expression in splenic cDCs from WT and LKB1$^{\Delta DC}$ mice. Each symbol represents an individual mouse. **e** Flow cytometry analysis of BODIPY expression in splenic DCs from WT and LKB1$^{\Delta DC}$ mice. **f** Statistics of basal oxygen consumption rate (OCR) and extracellular acidification rate (ECAR) (left) and OCR and ECAR of splenic DCs from WT and LKB1$^{\Delta DC}$ mice responding to the treatment of inhibitors oligomycin, FCCP (carbonyl cyanide p-trifluoromethoxyphenylhydrazone) and rotenone. Data are pooled from 4 experiments, with 2–4 mice per genotype in each experiment (in total 13 mice each genotype) and 3–8 technical replicates from each experiment. Each symbol represents a technical/biological replicate. **g** Flow cytometry analysis of cell size (FSC) of splenic DCs from WT and LKB1$^{\Delta DC}$ mice. Data in plots indicate the means ± s.e.m. Numbers in graphs indicate the mean fluorescence intensity. **P < 0.01, ***P < 0.001, ****P < 0.0001; two-tailed unpaired Student's *t*-test (**c**, **d**, **f**). Data are from two (**a**, **e**), one (**b**), at least three (**c**, **d**, **g**), or four (**f**) independent experiments

is generally considered to be reciprocally regulated,[53] our data suggest that both tTreg expansion and Th17 responses are restrained by DC LKB1 signaling. Specifically, DC-specific deletion of LKB1 does not affect DC development, but augments expression of DC maturational receptors, multiple cytokines and immunoregulatory molecules. Furthermore, loss of LKB1 results in lipid accumulation, upregulates glycolytic and mitochondrial metabolism, and induces aberrant mTOR activation in DCs. Suppressing mTOR signaling and IL-6 partially reversed the abnormal phenotypes of Treg expansion and IL-17 production,

respectively (Supplementary information, Fig. S6j). Thus, LKB1 acts as a signaling hub to establish metabolic and immune quiescence in DCs, thereby promoting immune homeostasis and anti-tumor immune responses.

DCs have been shown to control antigen-specific tTreg expansion and pTreg conversion from naïve CD4$^+$ T cells.[6,7] However, the signaling pathways utilized by DCs to control tTreg homeostasis remain uncertain. One striking phenotype of LKB1$^{\Delta DC}$ mice was the massively expanded Tregs, preferentially comprised of tTregs. The accelerated tumor growth in LKB1$^{\Delta DC}$
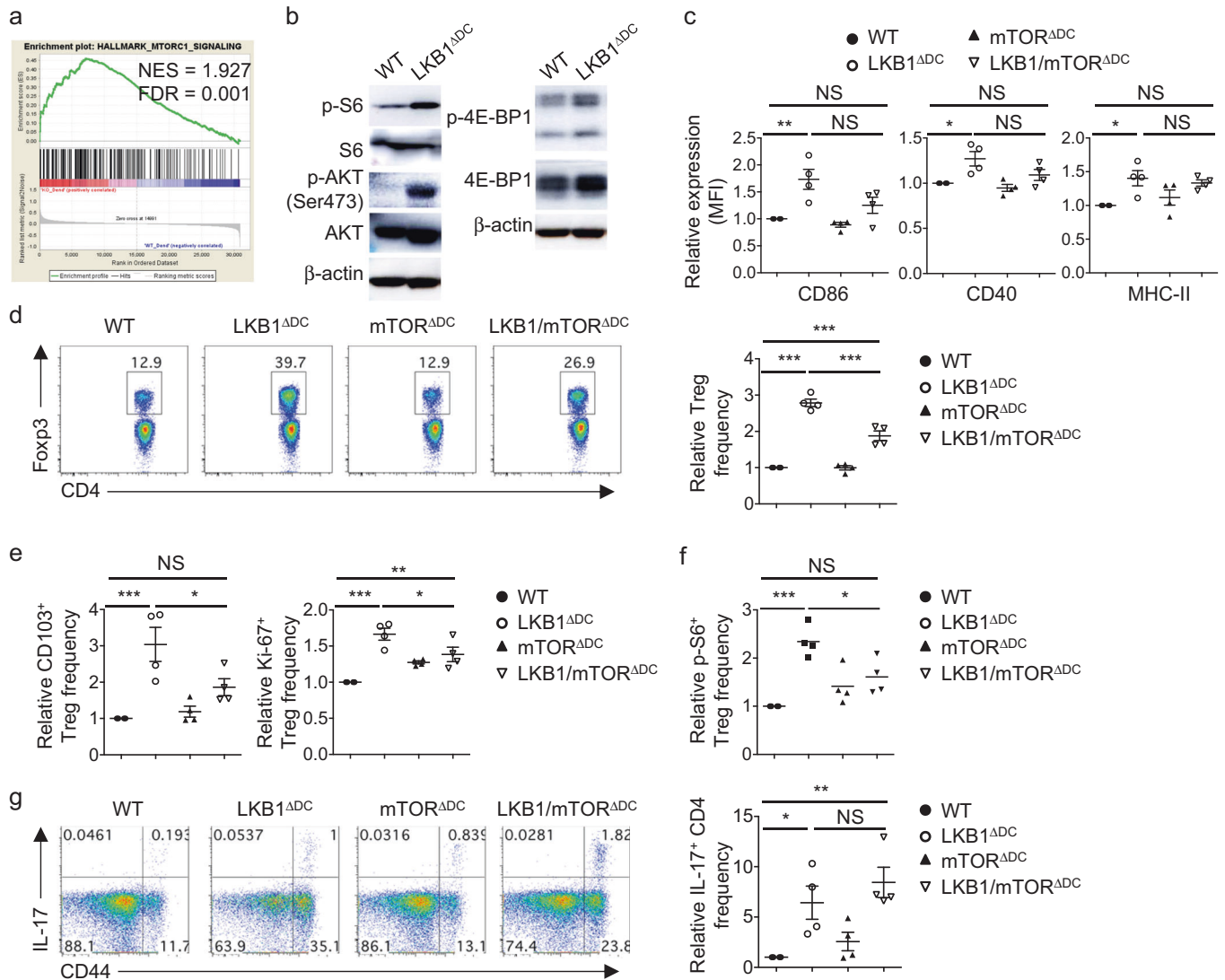
Fig. 7 LKB1 mediates DC quiescence and Treg control partially through restricting mTOR signaling. **a** Enrichment plot of the hallmark mTORC1 signaling in LKB1-deficient splenic DCs compared to WT DCs profiled using gene expression, identified by gene set enrichment analysis (GSEA). **b** Immunoblot analysis of splenic DCs from WT and LKB1$^{\Delta DC}$ mice. **c–g** WT, LKB1$^{\Delta DC}$, mTOR$^{\Delta DC}$, or LKB1/mTOR$^{\Delta DC}$ mice were analyzed. **c**, Statistics of CD86, CD40 and MHC-II expression on splenic DCs. **d** Flow cytometry analysis (left) and statistics (right) of splenic Foxp3$^+$CD4$^+$ Tregs. **e** Statistics of relative frequencies of CD103$^+$ and Ki-67$^+$ Tregs in the spleen. **f** Statistics of relative frequency of p-S6$^+$ Tregs in the spleen. **g** Flow cytometry analysis (left) and statistics (right) of IL-17 expression in splenic CD4$^+$ T cells. Data in plots indicate the means ± s.e.m; each symbol represents an individual mouse. Numbers in gates indicate percentage of cells. *NS* not significant; *$P < 0.05$, **$P <$ 0.01, ***$P < 0.001$; one-way ANOVA (**c–g**). Data are from two (**a**), three (**b**), or four (**c–g**) independent experiments

mice can be largely rescued by Treg depletion, highlighting the functional impacts of Tregs regulated by LKB1 signaling in DCs. The results from Treg adoptive transfer and co-culture experiments further reveal a direct role of LKB1 signaling in DCs in restraining excessive peripheral Treg expansion. Treg abundance depends upon IL-2 and the costimulatory molecule CD28, which interacts with CD86 and CD80 expressed by antigen-presenting cells including DCs.[54,55] LKB1 deficiency causes the upregulation of IL-2 and CD86 expression in DCs. In addition, LKB1-deficient DCs express higher levels of *Arg2*, *Ido1* and *Itgb8*, which can all contribute to Treg homeostasis in the periphery. We also observed enhanced Treg proliferation in the thymus of LKB1$^{\Delta DC}$ mice under steady state, and when co-cultured with LKB1-deficient thymic DCs in vitro. Furthermore, there was increased thymic Treg generation induced by DCs from LKB1$^{\Delta DC}$ mice, in line with the more abundant CD11b$^+$ thymic DCs[39] and increased co-stimulatory molecule expression that can promote Treg

generation.[50,56] Of note, we have observed efficient and specific deletion of *Stk11* in splenic and thymic DCs from LKB1$^{\Delta DC}$ mice and little non-specific deletion in macrophages or T cells, although we cannot fully exclude the possibility that additional cell types could be involved in vivo.[24] Mechanistically, LKB1 deletion results in aberrant upregulation of mTOR signaling, and deletion of mTOR partially rescues the increased tTreg phenotypes in LKB1$^{\Delta DC}$ mice, accompanied by dampened expression of CD86 and CD40 but not IL-2 in DCs. Although the signaling pathways in DCs mediating tTreg expansion are poorly understood, previous studies demonstrate that inhibition of mTOR activity in myeloid DCs promotes Foxp3 induction from naïve T cells (i.e. iTreg induction).[57–59] These observations are largely in line with our finding of a modest decrease of Foxp3 induction when co-culturing naïve T cells with LKB1-deficient DCs from MLN and spleen in vitro, which likely results from increased IL-6 production that can interfere with iTreg induction, although more work is needed to dissect the

underlying mechanisms. Collectively, LKB1 coordinates multiple pathways in DCs, in part by acting upon the LKB1-mTOR signaling axis, to keep Treg expansion under control to maintain immune homeostasis and protective anti-tumor immunity.

Th17 cells and Th17-associated cytokines have been shown to have both anti-tumorigenic and pro-tumorigenic functions in a highly context-dependent manner.[40] For instance, Th17 cells and IL-17 can mediate potent protective immunity in murine tumor models[42,43,60] and human cancer patients.[61,62] Interestingly, endogenous IL-17 has also been shown to exert pro-tumor function by increasing the proliferation and survival of tumor cells partially through activating the IL-6—STAT3 pathway.[44] We found that blocking IL-17Rα, IL-6 or STAT3 signaling partially inhibits tumor growth in LKB1[ΔDC] mice, revealing the roles of Th17 responses to altered tumor immunity in these mice. Nonetheless, Treg depletion produces more complete tumor suppression effects in LKB1[ΔDC] mice, suggesting that the contribution of Th17 responses to tumor growth phenotypes observed in these mice is likely associated with the markedly elevated Tregs, in line with the context-dependent role of Th17 cells in tumors.[40] Mechanistically, we found that LKB1-deficient DCs express increased levels of IL-6, and inhibition of IL-6 signaling via pharmacological or genetic approaches substantially rescues the increased Th17 phenotypes. Additionally, LKB1-deficient DCs express increased levels of TGFβ2 and integrin β8, which has been shown to activate TGFβ to promote Th17 cell development.[63,64] Thus, LKB1 suppresses several molecular pathways in DCs required for Th17 cell differentiation, with the control of IL-6 expression playing a more dominant effect.

Cellular metabolism has emerged as an essential regulator of DC development and function.[65] Quiescent DCs and activated DCs require different cellular metabolism to meet their bioenergetic and biosynthetic demands,[10,11] although little is known about the molecular determinant of DC metabolic quiescence. Of note, several positive regulators of DC metabolism have been reported in mediating DC-T cell interaction and in vivo adaptive immune responses, including PI3K-AKT, TBK1 and Hippo signaling.[12,13,66] Conversely, deletion of cholesterol efflux enzymes ABCA1 and ABCG1 in DCs results in accumulation of cholesterol and dysregulated T cell activation,[51] but the signaling pathways involved in the negative control of DC metabolism and DC–T cell interaction are uncertain. Here we identify LKB1 as a central negative regulator of cellular metabolism in DCs. Loss of LKB1 in DCs results in lipid accumulation and upregulated glycolysis. Since DC activation is frequently associated with upregulation of glycolysis,[13] these results support the loss of DC metabolic quiescence in the absence of LKB1. Additionally, oxygen consumption is enhanced in LKB1-deficient DCs, despite defective mitochondrial mass and potential (data not shown). Altogether, our study defines a central role of LKB1 in orchestrating anabolic programs in DCs to establish metabolic quiescence.

The serine and threonine kinase mTOR serves as a nutrient and energy sensor to integrate environmental cues and growth factor signaling and plays important roles in DC differentiation and function.[59] Once activated by growth factors or pattern recognition receptors, mTOR signaling activates many cellular processes in DCs, such as metabolism and protein synthesis, which control the expression of cytokines and surface molecules to regulate DC function. How mTOR activity is restricted remains poorly understood. We found that LKB1 deficiency activates mTOR signaling in DCs. Genetic deletion of mTOR activity ameliorates aberrant DC maturation but has no effect on LKB1-controled IL-2 expression, consistent with the partial rescue of the Treg accumulation phenotypes observed in LKB1[ΔDC] mice. Interestingly, LKB1 deletion upregulates both mTORC1 and mTORC2 activities, with a more pronounced increase in mTORC2 activity. Thus far, there is a limited understanding about the regulation and function of both mTOR complexes in DCs.[67] While modulation of either mTORC1 or

mTORC2 alone can alter DC-mediated T cell responses,[58,59,68–70] mTORC1 and mTORC2 signal through distinct downstream pathways and have extensive crosstalk.[71] Altogether, our study identifies that control of mTOR activity is an important, albeit partial, mechanism by which LKB1 functions in DCs to enforce DC quiescence and proper Treg responses. In contrast, the canonical pathways downstream of LKB1 signaling, including AMPK and HIF-1α signaling,[15,23,52] are largely dispensable for DC-mediated immune homeostasis. Future studies are warranted to dissect detailed biochemical pathways underlying the crosstalk between LKB1 and mTOR signaling, and the crosstalk between the two mTOR complexes, in DCs.

In summary, our study reveals a role of LKB1 in enforcing DC metabolic and immune quiescence to restrict excessive tTreg expansion and Th17 cell differentiation, and accordingly maintain normal immune homeostasis and protective anti-tumor immunity. Our findings suggest that DC-specific LKB1 signaling and metabolic regulation can be promising targets for modulating Treg and Th17 cell responses in cancer and immune-related diseases.

MATERIALS AND METHODS
Mice
C57BL/6, CD45.1[+], Rag1^{−/−}, OT-II, Thy1.1[+], Stk11[fl], Mtor[fl], Hif1a[fl], Prkaa1[fl], Prkaa2[fl], Foxp3[DTR], Il17ra^{−/−} and CD11c-Cre mice were purchased from The Jackson Laboratory. Foxp3[YFP-Cre] mice were a gift from A. Rudensky. All mice have been backcrossed to the C57BL/6 background. For mixed bone marrow chimera generation, bone marrow cells from WT or LKB1[ΔDC] CD45.2.2[+] mice were mixed with cells from CD45.1.2[+] mice at a 1:1 ratio and transferred into lethally irradiated CD45.1.1[+] mice, followed by reconstitution for 6–8 weeks, as described previously.[72] For complete Rag1^{−/−} bone marrow chimera generation, bone marrow cells from Rag1^{−/−} and LKB1[ΔDC]Rag1^{−/−} or Foxp3[DTR] and LKB1[ΔDC]Foxp3[DTR] mice were transferred into sublethally irradiated Rag1^{−/−} mice. All mice were kept in a specific pathogen-free facility in the Animal Resource Center at St. Jude Children's Research Hospital. Animal protocols were approved by the Institutional Animal Care and Use Committee of St. Jude Children's Research Hospital.

Cell purification and culture
Mouse spleen, thymus, and MLN were digested with Collagenase D (Worthington) and CD11c^{+} DCs were enriched using CD11c MicroBeads (Miltenyi Biotec) according to the manufacturer's instructions. Enriched cells were stained and sorted for CD11c^{+} DCs (CD11c^{+}MHC-II^{+}TCRβ^{−}CD19^{−}CD49b^{−}) or CD11c^{+}CD103^{+} MLN DCs (CD11c^{+}MHC-II^{+}TCRβ^{−}CD19^{−}CD49b^{−}CD103^{+}) on a Synergy or Reflection fluorescence activated cell sorter (Sony Biotechnology). Splenocytes were stained and sorted for CD11b^{+}F4/80^{+} macrophages. Lymphocytes from spleen and PLN were sorted for naïve CD4^{+} T cells (CD4^{+}CD62L^{hi}CD44^{lo}CD25^{−}), Tregs (CD25^{+}CD4^{+}) or Th17 cells (CD4^{+}TCRβ^{+}CD44^{hi}CCR6^{+}). The antibodies used for sorting were: anti-TCRβ (H57–597), anti-CD19 (eBio1D3 (1D3)), anti-CD49b (DX5), anti-CD11c (N418), anti-CD103 (2E7), anti-CD11b (M1/70), anti-F4/80 (BM8), anti-CD4 (RM4–5), anti-CD25 (PC61.5), anti-CD44 (IM7), CCR6 (29–2L17), and anti-CD62L (MEL-14) (all from eBioscience); and anti-MHC-II (M5/114.15.2, BioLegend). For splenic DC and periphery Treg cell co-culture, splenic DCs and CD25^{+}CD4^{+} T cells from spleen and PLN were mixed at the 1:10 ratio in the presence of 0.1 μg/mL anti-CD3 (2C11, Bio X Cell) and 20 U/mL IL-2, and cultured for 3 days. For thymic DC and thymic Treg co-culture to examine Treg proliferation, thymic DCs and CD4^{+}YFP-Foxp3^{+} thymocytes were mixed at the 1:10 ratio in the presence of 0.1 μg/mL anti-CD3 and 20 U/mL IL-2, and cultured for 3 days. For antibody blocking, 10 μg/mL anti-IL-2 (JES6-5H4) plus 10 μg/mL anti-CD25 (PC61, Bio X cell), 10 μg/mL

anti-IL-7 (M25, Bio X cell), anti-IL-15 (AF447, R&D) or 10 µg/mL anti-TGFβ (1D11, Bio X cell) were added to the cultures. Thymidine was added to the culture 7–8 h before harvest to measure cell proliferation. For in vitro Treg induction, MLN CD103$^+$ DCs and naïve OT-II CD4$^+$ T cells were mixed at the 1:10 ratio in the presence of 0.05 µg/mL OVA$_{323–339}$ peptide and cultured for 5 days, followed by flow cytometry analysis. For in vitro thymic Treg induction, thymic DCs were co-cultured with CD4$^+$CD8$^-$CD25$^-$YFP-Foxp3$^-$ thymocytes (tTreg precursors) at the 1:5 ratio in the presence of 10 ng/mL IL-7 (Peprotech) for 4 days. For in vitro Th17 cell differentiation, splenic DCs and naïve OT-II CD4$^+$ T cells were mixed at the 1:5 ratio in the presence of 50 µg/mL OVA$_{323–339}$ peptide and 100 ng/mL LPS, with or without 10 µg/mL anti-IL-6 (BD Biosciences) or 10 µg/mL anti-TGFβ (1D11), and cultured for 5 days, followed by flow cytometry analysis. For DC cytokine analysis, 1.5×10^5 DCs were stimulated with 100 ng/mL LPS in a 96-well round-bottom plate and culture supernatants were collected 2 days later for multiplex cytokine assays (Millipore).

Flow cytometry
Lymphocytes were harvested from the tissues by manual disruption or the colon lamina propria as previously described.[73] Flow cytometry was performed as described previously,[72] with the following antibodies: anti-TCRβ (H57–597), anti-CD44 (IM7), anti-CD103 (2E7), anti-ICOS (C398.4A), anti-CD25 (PC61.5), anti-CTLA-4, anti-PDCA-1 (eBio927), anti-CD19 (eBio1D3 (1D3)), anti-CD11c (N418), anti-CD40 (1C10), anti-MHC-II (M5/114.15.2), anti-CD80 (16-10A1), anti-CD86 (GL1), anti-CCR7 (4B12) (all from eBioscience); anti-neuropilin-1 (3E12), anti-CD11b (M1/70) (both from BioLegend); and anti-CD8 (53-6.7, Sony Biotechnology Inc). Intracellular Foxp3 (FJK-16s), anti-RORγt (B2D), anti-Ki-67 (SolA15), anti-Helios (22F6) (all from eBioscience), and anti-CTLA-4 (UC10-4B9; BioLegend) were analyzed by flow cytometry according to the manufacturer's instructions. For intracellular cytokine detection of IFNγ (XMG1.2), IL-17 (17B7, both from eBioscience), and IL-2 (JES6-5H4, BD Biosciences), cells were stimulated for 4 h with phorbol 12-myristate 13-acetate (PMA) and ionomycin in the presence of monensin before staining according to the manufacturer's instructions (BD Biosciences). BODIPY™ 493/503 (4,4-Difluoro-1,3,5,7,8-Pentamethyl-4-Bora-3a,4a-Diaza-s-Indacene) staining was performed according to the manufacturer's instructions (Invitrogen). For detection of phosphorylated signaling proteins, lymphocytes were rested in complete medium for 1 h and then fixed with Phosflow Lyse/Fix buffer, followed by permeabilization with Phosflow Perm buffer III (BD Biosciences) and staining with antibodies recognizing S6 phosphorylated at Ser235 and Ser236 (D57.2.2E; Cell Signaling Technology), 4E-BP1 phosphorylated at Thr37 and Thr46 (236B4; Cell Signaling Technology), LKB1 phosphorylated at Ser428 (Invitrogen), and p38 phosphorylated at Thr180 and Thr182 (236B4; Cell Signaling Technology). BrdU and active caspase-3 staining was performed according to the manufacturer's instruction (BD Biosciences). For DC caspase activity detection, splenocytes were stained with CaspACE FITC-VAD-FMK in situ marker according to the manufacturer's instructions (Promega). Flow cytometry data were acquired on LSRII or LSR Fortessa (BD Biosciences) and analyzed using FlowJo software (Tree Star).

Tumor model
MC38 colon adenocarcinoma cells or MC38-EGFR cells were cultured in DMEM supplemented with 10% (vol/vol) FBS and 1% (vol/vol) penicillin-streptomycin. B16-OVA cells were cultured in RPMI 1640 medium supplemented with 10% (vol/vol) FBS and 1% (vol/vol) penicillin-streptomycin. Mice were injected subcutaneously with 5×10^5 MC38 tumor cells, 5×10^6 MC38-EGFR cells or 3×10^5 B16-OVA cells in the right flank. Tumors were measured regularly with calipers. Tumor volumes were calculated using the

formula: length × width × width × π/6. For the LKB1$^{\Delta DC}$Foxp3^{DTR} chimera MC38 tumor model, the chimeras were treated with 25 µg/kg DT i.p. every 4 days started from day −1, for a total of 3 injections. For the Stat3 inhibitor JSI-124 (cucurbitacin I, EMD Millipore) treatment, the mice were immunized with MC38 tumor cells at day 0, and randomized to control or treatment group at day 4 for injection of vehicle or 1 mg/kg/d JSI-124 i.p. consecutively for 13 days. To prepare tumor infiltrating lymphocytes, tumor tissues were excised, minced and digested with 0.5 mg/mL Collagenase IV (Roche) + 200 U/mL DNase I (Sigma) for 1 h at 37 °C. Tumor infiltrating lymphocytes were then isolated by density-gradient centrifugation over Percoll (Life Technologies).

Antigen challenge
Naïve CD4$^+$ T cells from OT-II TCR-transgenic mice (Thy1.1$^+$) were sorted and transferred into WT and LKB1$^{\Delta DC}$ mice. Twenty-four hours later, the mice were injected s.c. in the footpad with OVA$_{323–339}$ (100 µg) emulsified with the complete Freund's adjuvant (CFA; Difco). At day 7 after immunization, popliteal draining lymph node (DLN) cells were isolated for further analyses. In the model of oral antigen stimulation, after adoptive transfer of naïve OT-II CD4$^+$ T cells, mice were fed with water supplemented with 20 mg/mL OVA protein (Grade VI; Sigma) for a total of 5 days for analysis.[72] For KLH response, KLH (Sigma, 0.5 mg/mL) was emulsified with 0.5 mg/mL CFA and injected s.c. in the footpad (100 µL each mouse). Seven days later, popliteal DLN cells and splenocytes were isolated and stimulated with 10 µg/mL KLH for day 2 RNA, or with 0, 1, 10, 100 µg/mL KLH for day 3 cytokine secretion assays. Cytokine secretion was measured by multiplex cytokine assays (Millipore).

Metabolic assays via Seahorse
Oxygen consumption rates (OCR) and extracellular acidification rates (ECAR) were measured in XF media under basal conditions and in response to 1 µM oligomycin, 1.5 µM fluoro-carbonyl cyanide phenylhydrazone (FCCP) and 500 nM rotenone using an XF96 Extracellular Flux Analyzer (EFA) (Seahorse Bioscience).

RNA and immunoblot analysis
Real-time PCR analysis was performed as previously described with primers and probe sets from Applied Biosystems, or using Power SYBR Green Master Mix from Life Technologies.[74] Immunoblots were performed and quantified as described previously,[72] using the following antibodies: p-LKB1 (Ser428; C67A3), LKB1 (D60C5), p-S6 (Ser235/236) (2F9), p-4E-BP1 (Thr37/46) (236B4), p-AKT (Ser473) (D9E), S6 (5G10), 4E-BP1 (53H11) (236B4), AKT (#9272) (all from Cell Signaling Technology) and β-actin (Sigma).

Immunofluorescence
Lymph nodes were fixed in 2% paraformaldehyde, 0.1% Triton-100 and 1% DMSO for 24 h prior to incubation in blocking buffer comprised of PBS containing 2% bovine serum albumin and 5% donkey serum for an additional 24 h. Tissues were subsequently incubated in blocking buffer containing 1 µg/mL of AF488-conjugated anti-CD11c (clone N418), PE-conjugated anti-Foxp3 (clone FJK-16s) and AF647-conjugated MHC-II (clone M5/114.15.2) for 72 h at 4 °C with shaking. Tissues were washed with 3 changes of blocking buffer for 24 h prior to embedding in tissue freezing medium. Tissues were cryosectioned and mounted with prolong diamond antifade mounting media (ThermoFisher). High resolution images were acquired using a Marianis spinning disk confocal microscope (Intelligent Imaging Innovations) equipped with a 40× 1.3NA objective and EMCCD camera. Images were subsequently analyzed using Imaris software (Bitplane), where the center of mass was determined for each Foxp3 or CD11c object, followed by positional analysis to determine the frequency of objects considered to be interacting (distance between centers less than 5 µm) or non-interacting (distance between centers greater than 5 µm).

In vitro Treg suppression assays

For analysis of Treg suppression in vitro, CD25⁺CD4⁺ Tregs, isolated from the spleen and PLN of WT and LKB1^ΔDC mice, were cultured with WT naïve CD4⁺ T cells and irradiated splenocytes as antigen-presenting cells in the presence of 0.05 µg/mL anti-CD3 for three days, and the incorporation of [³H]-thymidine was assessed as previously described.[34]

Adoptive transfer of Tregs and in vivo anti-IL-2 blockade

Sorted CD25⁺CD4⁺ Tregs, isolated from the spleen and PLN of CD45.1⁺ mice, were incubated in Click's medium with 5% FBS and 3.5 µM CellTrace Violet (CellTrace, Life Technologies) at 37 °C for 25 min, followed by extensive washes. The cells were then transferred into WT and LKB1^ΔDC mice intravenously for Treg proliferation analysis seven days later. For anti-IL-2 blockade, the mice were treated with isotype control or anti-IL-2 antibodies (JES6-5H4, Bio X cell) i.p. at days −1, 2 and 5.[75]

Whole proteome profiling by multiplex TMT-LC/LC-MS/MS

Protein extraction, digestion, labeling and pooling. Whole proteome profiling was performed as recently described.[76,77] Splenic DCs were sorted from WT and LKB1^ΔDC mice as described above. Cells were washed twice with ice cold PBS and cell pellets from 4 samples ($n = 2$ per genotype, with each DC sample pooled from 2–3 mice) were lysed in fresh lysis buffer (50 mM HEPES, pH 8.5, 8 M urea and 0.5% sodium deoxycholate) respectively. The protein concentration of lysate was quantified by BCA protein assay (Thermo Fisher Scientific). Proteins (100 µg) from each sample were digested with trypsin (Promega, 1:50 w/w) followed by peptide desalting, and drying by speedvac. Each sample was then resuspended in 50 mM HEPES, pH 8.5, and labeled with TMT reagents following the manufacturer's instruction. Then, the TMT-labeled samples were equally mixed.

Offline basic pH reverse phase liquid chromatography. The mixture of the TMT-labeled samples was desalted, dried and solubilized in 60 µL of buffer A (10 mM ammonium formate, pH 8) and separated on an XBridge C18 column (3.5 µm particle size, 4.6 mm × 25 cm, Waters) into 39 fractions with an 88 min gradient from 15 to 45% buffer B (95% acetonitrile, 10 mM ammonium formate, pH 8, flow rate of 0.4 mL/min). Each fraction was dried for whole proteome analysis.

Acidic pH reverse phase liquid chromatography coupled with tandem MS. The analysis was performed based on our optimized platform.[78] For whole proteome analysis, the dried peptides were reconstituted in 5% formic acid, loaded on a reverse phase column (75 µm × 30 cm, 1.9 µm C18 resin (Dr. Maisch GmbH, Germany)) interfaced with a Q-Exactive HF mass spectrometer (ThermoFisher Scientific). Peptides were eluted by 12–36% buffer B gradient in 2.5 h (buffer A: 0.2% formic acid, 3% DMSO; buffer B: buffer A plus 67% acetonitrile, flow rate of 0.25 µL/min). The column was heated at 65 °C by a butterfly portfolio heater (Phoenix S&T) to reduce backpressure. Mass spectrometer was operated in data-dependent mode with a survey scan in Orbitrap (60,000 resolution, 1×10^6 AGC target and 50 ms maximal ion time) and 20 MS/MS high resolution scans (60,000 resolution, 1×10^5 AGC target, 105 ms maximal ion time, HCD, 35 normalized collision energy, 1.0 m/z isolation window, and 20 s dynamic exclusion). All data are shown in Supplementary information, Table S1.

Proteomics data analysis. The analysis was performed by the JUMP program, a newly developed hybrid search engine that combines tag scoring and pattern match scoring to improve sensitivity and specificity, and has been used in the data processing of numerous publications.[66,76,79] Briefly, acquired MS/MS raw files were converted into mzXML format and searched by the JUMP algorithm against a composite target/decoy database to estimate false discover rate (FDR). The target protein database was downloaded from the Uniprot mouse database (52,490 protein entries) and the decoy protein database was generated by reversing all target protein sequences. Searches were performed with 10 ppm mass tolerance for both precursor ions and product ions, fully tryptic restriction, two maximal missed cleavages and the assignment of *a*, *b*, and *y* ions. TMT tags on lysine residues and peptide N termini (+229.16293 Da) and carbamidomethylation of cysteine residues (+57.02146 Da) were used for static modifications and oxidation of methionine residues (+15.99491 Da) were used for dynamic modification. The assigned peptides were filtered by mass accuracy, minimal peptide length, matching scores, charge state and trypticity to reduce protein FDR to below 1%.

TMT-based protein quantification. The analysis was performed by JUMP software suite as previously reported.[76] In brief, TMT reporter ion intensities of each PSM were extracted and the PSMs with very low intensity were removed. The raw intensities were then corrected based on isotopic distribution of each labeling reagent and loading bias. The mean-centered intensities across samples were calculated and protein relative intensities were derived by averaging related PSMs. Finally, protein absolute intensities were determined by multiplying the relative intensities by the grand-mean of three most highly abundant PSMs.

Gene-expression profiling and bioinformatics analysis

Splenic DCs ($n = 4$ or $n = 3$ per genotype from 2 independent experiments) and peripheral CD4⁺CD25⁺ Tregs ($n = 4$ for WT, $n = 3$ for LKB1^ΔDC mice) were isolated from WT and LKB1^ΔDC mice as described above. RNA was obtained with a RNeasy Micro Kit according to the manufacturer's instructions (Qiagen). RNA samples were then analyzed with the Mouse Gene 2.0 ST Signals array. Differentially expressed transcripts were identified by ANOVA (Partek Genomics Suite version 6.5), and the Benjamini-Hochberg method was used to estimate the FDR. GSEA of hallmark pathways from these microarray samples or proteomics samples was performed as previously described.[34] Microarray data are available via Gene Expression Omnibus under accession number GSE128475.

Statistical analysis

P values were calculated by Mann-Whitney test, two-tailed unpaired Student's *t* test, and one-way or two-way ANOVA using GraphPad Prism, unless otherwise noted. $P < 0.05$ was considered as significant. Pearson correlation coefficient was performed for correlation analysis. All error bars represent the s.e.m.

AUTHOR CONTRIBUTIONS

Y.W. designed, performed, and analyzed experiments and wrote the manuscript; X.D. performed biochemical experiments; J.W. performed tumor study; L.L., H.T., and J.P. performed and analyzed proteomics assays; C.G. performed imaging assay, Y.D., C.Q., G.N., and J.Y. performed bioinformatics analyses; Y-X.F. provided crucial reagents and scientific insight; H.C. designed experiments, wrote the manuscript, and provided overall direction.

ADDITIONAL INFORMATION

Supplementary information accompanies this paper at https://doi.org/10.1038/s41422-019-0157-4.

Competing interests: The authors declare that they have no conflict of interest.

REFERENCES

1. Merad, M., Sathe, P., Helft, J., Miller, J. & Mortha, A. The dendritic cell lineage: ontogeny and function of dendritic cells and their subsets in the steady state and the inflamed setting. *Annu. Rev. Immunol.* **31**, 563–604 (2013).
2. Durai, V. & Murphy, K. M. Functions of murine dendritic cells. *Immunity* **45**, 719–736 (2016).
3. Meredith, M. M. et al. Expression of the zinc finger transcription factor zDC (Zbtb46, Btbd4) defines the classical dendritic cell lineage. *J. Exp. Med.* **209**, 1153–1165 (2012).
4. Ohnmacht, C. et al. Constitutive ablation of dendritic cells breaks self-tolerance of CD4 T cells and results in spontaneous fatal autoimmunity. *J. Exp. Med.* **206**, 549–559 (2009).
5. Birnberg, T. et al. Lack of conventional dendritic cells is compatible with normal development and T cell homeostasis, but causes myeloid proliferative syndrome. *Immunity* **29**, 986–997 (2008).
6. Iberg, C. A., Jones, A. & Hawiger, D. Dendritic cells as inducers of peripheral tolerance. *Trends Immunol.* **38**, 793–804 (2017).
7. Audiger, C., Rahman, M. J., Yun, T. J., Tarbell, K. V. & Lesage, S. The importance of dendritic cells in maintaining immune tolerance. *J. Immunol.* **198**, 2223–2231 (2017).
8. Abbas, A. K. et al. Regulatory T cells: recommendations to simplify the nomenclature. *Nat. Immunol.* **14**, 307–308 (2013).
9. Darrasse-Jeze, G. et al. Feedback control of regulatory T cell homeostasis by dendritic cells in vivo. *J. Exp. Med.* **206**, 1853–1862 (2009).
10. Pearce, E. J. & Everts, B. Dendritic cell metabolism. *Nat. Rev. Immunol.* **15**, 18–29 (2015).
11. O'Neill, L. A. & Pearce, E. J. Immunometabolism governs dendritic cell and macrophage function. *J. Exp. Med.* **213**, 15–23 (2016).
12. Everts, B. et al. TLR-driven early glycolytic reprogramming via the kinases TBK1-IKKvarepsilon supports the anabolic demands of dendritic cell activation. *Nat. Immunol.* **15**, 323–332 (2014).
13. Krawczyk, C. M. et al. Toll-like receptor-induced changes in glycolytic metabolism regulate dendritic cell activation. *Blood* **115**, 4742–4749 (2010).
14. Hemminki, A. et al. A serine/threonine kinase gene defective in Peutz-Jeghers syndrome. *Nature* **391**, 184–187 (1998).
15. Shackelford, D. B. & Shaw, R. J. The LKB1-AMPK pathway: metabolism and growth control in tumour suppression. *Nat. Rev. Cancer* **9**, 563–575 (2009).
16. Gan, B. et al. Lkb1 regulates quiescence and metabolic homeostasis of haematopoietic stem cells. *Nature* **468**, 701–704 (2010).
17. Gurumurthy, S. et al. The Lkb1 metabolic sensor maintains haematopoietic stem cell survival. *Nature* **468**, 659–663 (2010).
18. Nakada, D., Saunders, T. L. & Morrison, S. J. Lkb1 regulates cell cycle and energy metabolism in haematopoietic stem cells. *Nature* **468**, 653–658 (2010).
19. He, N. et al. Metabolic control of regulatory T cell (Treg) survival and function by Lkb1. *Proc. Natl Acad. Sci. USA* **114**, 12542–12547 (2017).
20. Yang, K. et al. Homeostatic control of metabolic and functional fitness of Treg cells by LKB1 signalling. *Nature* **548**, 602–606 (2017).
21. Wu, D. et al. Lkb1 maintains Treg cell lineage identity. *Nat. Commun.* **8**, 15876 (2017).
22. Poffenberger, M. C. et al. LKB1 deficiency in T cells promotes the development of gastrointestinal polyposis. *Science* **361**, 406–411 (2018).
23. MacIver, N. J. et al. The liver kinase B1 is a central regulator of T cell development, activation, and metabolism. *J. Immunol.* **187**, 4187–4198 (2011).
24. Caton, M. L., Smith-Raska, M. R. & Reizis, B. Notch-RBP-J signaling controls the homeostasis of CD8- dendritic cells in the spleen. *J. Exp. Med.* **204**, 1653–1664 (2007).
25. Kim, J. M., Rasmussen, J. P. & Rudensky, A. Y. Regulatory T cells prevent catastrophic autoimmunity throughout the lifespan of mice. *Nat. Immunol.* **8**, 191–197 (2007).
26. Thornton, A. M. et al. Expression of Helios, an Ikaros transcription factor family member, differentiates thymic-derived from peripherally induced Foxp3+ T regulatory cells. *J. Immunol.* **184**, 3433–3441 (2010).
27. Weiss, J. M. et al. Neuropilin 1 is expressed on thymus-derived natural regulatory T cells, but not mucosa-generated induced Foxp3+ T reg cells. *J. Exp. Med.* **209**, 1723–1742 (2012). S1721.
28. Yadav, M. et al. Neuropilin-1 distinguishes natural and inducible regulatory T cells among regulatory T cell subsets in vivo. *J. Exp. Med.* **209**, 1713–1722 (2012). S1711-1719.
29. Gottschalk, R. A., Corse, E. & Allison, J. P. Expression of Helios in peripherally induced Foxp3+ regulatory T cells. *J. Immunol.* **188**, 976–980 (2012).
30. Ohnmacht, C. et al. MUCOSAL IMMUNOLOGY. The microbiota regulates type 2 immunity through RORgammat(+) T cells. *Science* **349**, 989–993 (2015).
31. Sefik, E. et al. MUCOSAL IMMUNOLOGY. Individual intestinal symbionts induce a distinct population of RORgamma(+) regulatory T cells. *Science* **349**, 993–997 (2015).
32. Sun, C. M. et al. Small intestine lamina propria dendritic cells promote de novo generation of Foxp3 T reg cells via retinoic acid. *J. Exp. Med.* **204**, 1775–1785 (2007).
33. Huang, G., Wang, Y., Shi, L. Z., Kanneganti, T. D. & Chi, H. Signaling by the phosphatase MKP-1 in dendritic cells imprints distinct effector and regulatory T cell fates. *Immunity* **35**, 45–58 (2011).
34. Zeng, H. et al. mTORC1 couples immune signals and metabolic programming to establish T(reg)-cell function. *Nature* **499**, 485–490 (2013).
35. Procaccini, C. et al. An oscillatory switch in mTOR kinase activity sets regulatory T cell responsiveness. *Immunity* **33**, 929–941 (2010).
36. Malek, T. R. & Castro, I. Interleukin-2 receptor signaling: at the interface between tolerance and immunity. *Immunity* **33**, 153–165 (2010).
37. Granucci, F. et al. Inducible IL-2 production by dendritic cells revealed by global gene expression analysis. *Nat. Immunol.* **2**, 882–888 (2001).
38. Toomer, K. H. & Malek, T. R. Cytokine signaling in the development and homeostasis of regulatory T cells. *Cold Spring Harb. Perspect. Biol.* **10**, pii: a028597 (2018).
39. Proietto, A. I. et al. Dendritic cells in the thymus contribute to T-regulatory cell induction. *Proc. Natl Acad. Sci. USA* **105**, 19869–19874 (2008).
40. Zou, W. & Restifo, N. P. T(H)17 cells in tumour immunity and immunotherapy. *Nat. Rev. Immunol.* **10**, 248–256 (2010).
41. Patel, D. D. & Kuchroo, V. K. Th17 cell pathway in human immunity: lessons from genetics and therapeutic interventions. *Immunity* **43**, 1040–1051 (2015).
42. Kryczek, I., Wei, S., Szeliga, W., Vatan, L. & Zou, W. Endogenous IL-17 contributes to reduced tumor growth and metastasis. *Blood* **114**, 357–359 (2009).
43. Martin-Orozco, N. et al. T helper 17 cells promote cytotoxic T cell activation in tumor immunity. *Immunity* **31**, 787–798 (2009).
44. Wang, L. et al. IL-17 can promote tumor growth through an IL-6-Stat3 signaling pathway. *J. Exp. Med.* **206**, 1457–1464 (2009).
45. Puccetti, P. & Grohmann, U. IDO and regulatory T cells: a role for reverse signalling and non-canonical NF-kappaB activation. *Nat. Rev. Immunol.* **7**, 817–823 (2007).
46. Travis, M. A. et al. Loss of integrin alpha(v)beta8 on dendritic cells causes autoimmunity and colitis in mice. *Nature* **449**, 361–365 (2007).
47. McGovern, N. et al. Human fetal dendritic cells promote prenatal T-cell immune suppression through arginase-2. *Nature* **546**, 662–666 (2017).
48. Dohler, A. et al. RelB(+) steady-atate migratory dendritic cells control the peripheral pool of the natural Foxp3(+) regulatory T cells. *Front Immunol.* **8**, 726 (2017).
49. Platt, A. M. & Randolph, G. J. Dendritic cell migration through the lymphatic vasculature to lymph nodes. *Adv. Immunol.* **120**, 51–68 (2013).
50. Pletinckx, K., Dohler, A., Pavlovic, V. & Lutz, M. B. Role of dendritic cell maturity/costimulation for generation, homeostasis, and suppressive activity of regulatory T cells. *Front Immunol.* **2**, 39 (2011).
51. Westerterp, M. et al. Cholesterol accumulation in dendritic cells links the inflammasome to acquired immunity. *Cell Metab.* **25**, 1294–1304 e1296 (2017).
52. Faubert, B. et al. Loss of the tumor suppressor LKB1 promotes metabolic reprogramming of cancer cells via HIF-1alpha. *Proc. Natl Acad. Sci. USA* **111**, 2554–2559 (2014).
53. Zhu, J., Yamane, H. & Paul, W. E. Differentiation of effector CD4 T cell populations (*). *Annu. Rev. Immunol.* **28**, 445–489 (2010).
54. Salomon, B. et al. B7/CD28 costimulation is essential for the homeostasis of the CD4+CD25+ immunoregulatory T cells that control autoimmune diabetes. *Immunity* **12**, 431–440 (2000).
55. Bar-On, L., Birnberg, T., Kim, K. W. & Jung, S. Dendritic cell-restricted CD80/86 deficiency results in peripheral regulatory T-cell reduction but is not associated with lymphocyte hyperactivation. *Eur. J. Immunol.* **41**, 291–298 (2011).
56. Yamazaki, S. et al. Direct expansion of functional CD25+CD4+ regulatory T cells by antigen-processing dendritic cells. *J. Exp. Med.* **198**, 235–247 (2003).
57. Rosborough, B. R. et al. Murine dendritic cell rapamycin-resistant and rictor-independent mTOR controls IL-10, B7-H1, and regulatory T-cell induction. *Blood* **121**, 3619–3630 (2013).
58. Thomson, A. W., Turnquist, H. R. & Raimondi, G. Immunoregulatory functions of mTOR inhibition. *Nat. Rev. Immunol.* **9**, 324–337 (2009).
59. Sukhbaatar, N., Hengstschlager, M. & Weichhart, T. mTOR-mediated regulation of dendritic cell differentiation and function. *Trends Immunol.* **37**, 778–789 (2016).
60. Muranski, P. et al. Th17 cells are long lived and retain a stem cell-like molecular signature. *Immunity* **35**, 972–985 (2011).

61. Kryczek, I. et al. Phenotype, distribution, generation, and functional and clinical relevance of Th17 cells in the human tumor environments. *Blood* **114**, 1141–1149 (2009).

62. Kryczek, I. et al. Human TH17 cells are long-lived effector memory cells. *Sci. Transl. Med* **3**, 104ra100 (2011).

63. Melton, A. C. et al. Expression of alphavbeta8 integrin on dendritic cells regulates Th17 cell development and experimental autoimmune encephalomyelitis in mice. *J. Clin. Invest*. **120**, 4436–4444 (2010).

64. Acharya, M. et al. alphav Integrin expression by DCs is required for Th17 cell differentiation and development of experimental autoimmune encephalomyelitis in mice. *J. Clin. Invest.* **120**, 4445–4452 (2010).

65. Du, X., Chapman, N. M. & Chi, H. Emerging roles of cellular metabolism in regulating dendritic cell subsets and function. *Front Cell Dev. Biol.* **6**, 152 (2018).

66. Du, X. et al. Hippo/Mst signalling couples metabolic state and immune function of CD8alpha(+) dendritic cells. *Nature* **558**, 141–145 (2018).

67. Sinclair, C. et al. mTOR regulates metabolic adaptation of APCs in the lung and controls the outcome of allergic inflammation. *Science* **357**, 1014–1021 (2017).

68. Weichhart, T. et al. The TSC-mTOR signaling pathway regulates the innate inflammatory response. *Immunity* **29**, 565–577 (2008).

69. Amiel, E. et al. Inhibition of mechanistic target of rapamycin promotes dendritic cell activation and enhances therapeutic autologous vaccination in mice. *J. Immunol.* **189**, 2151–2158 (2012).

70. Raich-Regue, D. et al. mTORC2 deficiency in myeloid dendritic cells enhances their allogeneic Th1 and Th17 stimulatory ability after TLR4 ligation in vitro and in vivo. *J. Immunol.* **194**, 4767–4776 (2015).

71. Saxton, R. A. & Sabatini, D. M. mTOR signaling in growth, metabolism, and disease. *Cell* **168**, 960–976 (2017).

72. Wang, Y. et al. Transforming growth factor beta-activated kinase 1 (TAK1)-dependent checkpoint in the survival of dendritic cells promotes immune homeostasis and function. *Proc. Natl Acad. Sci. USA* **109**, E343–E352 (2012).

73. Chapman, N. M. et al. mTOR coordinates transcriptional programs and mitochondrial metabolism of activated Treg subsets to protect tissue homeostasis. *Nat. Commun.* **9**, 2095 (2018).

74. Wang, Y. et al. Tuberous sclerosis 1 (Tsc1)-dependent metabolic checkpoint controls development of dendritic cells. *Proc. Natl Acad. Sci. USA* **110**, E4894–E4903 (2013).

75. Smigiel, K. S. et al. CCR7 provides localized access to IL-2 and defines homeostatically distinct regulatory T cell subsets. *J. Exp. Med.* **211**, 121–136 (2014).

76. Tan, H. et al. Integrative pProteomics and phosphoproteomics profiling reveals dynamic signaling networks and bioenergetics pathways underlying T cell activation. *Immunity* **46**, 488–503 (2017).

77. Bai, B. et al. Deep profiling of proteome and phosphoproteome by isobaric labeling, extensive liquid chromatography, and mass spectrometry. *Methods Enzymol.* **585**, 377–395 (2017).

78. Wang, H. et al. Systematic optimization of long gradient chromatography mass spectrometry for deep analysis of brain proteome. *J. Proteome Res* **14**, 829–838 (2015).

79. Wang, X. et al. JUMP: a tag-based database search tool for peptide identification with high sensitivity and accuracy. *Mol. Cell Proteom.* **13**, 3663–3673 (2014).